The seasonal cycle of atmospheric heating and temperature

Aaron Donohoe *

Massachusetts Institute of Technology, Cambridge, Massachusetts

David S. Battisti

Department of Atmospheric Sciences, University of Washington, Seattle, Washington

(Manuscript submitted September 28, 2012)

* *Corresponding author address:* Aaron Donohoe, Massachusetts Institute of Technology, Dept. of Earth, Atmospheric and Planetary Sciences, Room Number 54-918, 77 Massachusetts Avenue, Cambridge, MA 02139-4307.

E-mail: thedhoe@mit.edu

ABSTRACT

The seasonal cycle of the heating of the atmosphere is divided into a component due to direct solar absorption in the atmosphere, and a component due to the flux of energy from the surface to the atmosphere via latent, sensible, and radiative heat fluxes. Both observations and coupled climate models are analyzed. The vast majority of the seasonal heating of the Northern extratropics (67% in the observations and 78% in the model average) is due to atmospheric shortwave absorption. In the southern extratropics, the seasonal heating of the atmosphere is entirely due to atmospheric shortwave absorption in both the observations and the models, and the surface heat flux opposes the seasonal heating of the atmosphere. The seasonal cycle of atmospheric temperature is surface amplified in the northern extratropics and nearly barotropic in the southern hemisphere; in both cases, the vertical profile of temperature reflects the source of the seasonal heating.

In the northern extratropics, the seasonal cycle of atmospheric heating over land differs markedly from that over the ocean. Over the land, the surface energy fluxes compliment the driving absorbed shortwave flux; over the ocean they oppose the absorbed shortwave flux. This gives rise to large seasonal differences in the temperature of the atmosphere over land and ocean. Downgradient temperature advection by the mean westerly winds damps the seasonal cycle of heating of the atmosphere over the land and amplifies it over the ocean. The seasonal cycle in the zonal energy transport is 4.1 PW.

Finally, we examine the change in the seasonal cycle of atmospheric heating in 11 CMIP3 models due to a doubling of atmospheric carbon dioxide from pre-industrial concentrations. We find the seasonal heating of the troposphere is everywhere enhanced by increased shortwave absorption by water vapor; it is reduced where sea ice has been replaced by ocean which

increases the effective heat storage reservoir of the climate system and thereby reduces the seasonal magnitude of energy fluxes between the surface and the atmosphere. As a result, the seasonal amplitude of temperature increases in the upper troposphere (where atmospheric shortwave absorption increases) and decreases at the surface (where the ice melts).

1. Introduction

Averaged annually and globally, the atmosphere receives approximately two thirds of its energy input from upward energy fluxes from the surface (longwave, sensible, and latent heat fluxes) and the remaining one third from direct atmospheric absorption of shortwave radiation (Kiehl and Trenberth 1997; Trenberth et al. 2009). This result follows from the fact that (A) the atmosphere is more transparent than absorbing in the shortwave bands resulting in more shortwave radiation absorbed at the surface than within the atmosphere itself (Gupta et al. 1999), and (B) the surface is in energetic equilibrium (provided that energy is not accumulating in the system) such that the net shortwave radiation absorbed at the surface is balanced by an upward energy flux toward the atmosphere (Dines 1917). As a result, in the annual average, the atmosphere is heated from below (by surface fluxes) rather from above (from atmospheric shortwave absorption). Energy is primarily redistributed vertically from the input region at the surface to the region of net radiative cooling aloft by convection (Held et al. 1993).

The seasonal input of energy into the atmosphere has received less attention in the literature and is not subject to the same constraints imposed on the annual average. Specifically, the oceans can store large quantities of energy in the annual cycle (Fasullo and Trenberth 2008a) and there is therefore no requirement that the seasonal variations in net shortwave absorption at the surface be balanced by an upward energy flux toward the atmosphere. Consequently, although the atmosphere is more shortwave transparent than shortwave absorbing during all seasons, there is no *a prioir* requirement that the atmosphere be heated from below rather than above in the annual cycle. The relative contributions of atmospheric

shortwave absorption and surface heating to the seasonal heating of the atmosphere is an unresolved issue in climate dynamics and it is the focus of this study.

The seasonal flow of energy in the climate system has been thoroughly documented by Trenberth and Stepaniak (2004) and Fasullo and Trenberth (2008b). There, it was demonstrated that the large seasonal variations in shortwave radiation at the top of the atmosphere (TOA) were primarily balanced by an energy flux into the ocean. In this regard, the seasonal input of energy into the the atmospheric column is the residual of two large terms: the net shortwave flux at the TOA and the net energy flux through the surface. To better elucidate the seasonal heating of the atmosphere, we take the unconventional approach of dividing the surface energy flux into solar and non-solar components. This choice is motivated by the fact that the solar flux through the surface is an exchange of energy between the Sun and the surface whereas the non-solar surface energy flux represents an energy exchange between the surface and the atmosphere that (potentially) serves to heat the atmosphere seasonally. Our framework shows that the vast majority of the seasonal heating of the atmosphere is due to atmospheric absorption of shortwave radiation as opposed to seasonal variations in the upward energy flux from the surface to the atmosphere.

The division of seasonal atmospheric heating into upward surface fluxes and shortwave atmospheric absorption has implications for the vertical structure of the seasonal temperature response, the hydrological cycle, the temporal phasing of the seasonal cycle and, the change in seasonality due to global warming. Heating the air column from below destabilizes the air column often triggering convection and a vertical temperature profile at the adiabatic lapse rate (Manabe and Wetherald 1967). In contrast, heating the atmosphere at an upper level stabilizes the air column and results in a temperature response that mimics

the radiative heating profile (Fels 1985). We demonstrate that, throughout most for the domain, the annual cycle of temperature has a vertical profile that reflects the distribution of shortwave atmospheric heating. The partitioning of atmospheric heating into surface fluxes and atmospheric absorption is also useful for understanding the strength of the hydrological cycle which is intimately connected to the upward surface fluxes (Takahashi 2009).

The phase of the seasonal cycle of temperature within the atmosphere is also dictated by the heating source. For example, the upward energy fluxes from the surface to the atmosphere lag the insolation (especially over the ocean) because the surface must first heat up before it can flux energy to the atmosphere. In contrast, shortwave absorption in the atmosphere is phase locked to the insolation. Therefore, an atmosphere that is heated by shortwave absorption will have a phase lead in the seasonal cycle of temperature relative to an atmosphere that is heated by surface fluxes.

Changes in the seasonal heating of the atmosphere due to increasing CO_2 concentrations will have a direct impact on the seasonal cycle of atmospheric temperatures. The source of the seasonal heating of the atmosphere is anticipated to change with global warming as a consequence of (1) reduced sea ice extent leading to a larger effective surface heat capacity (Dwyer et al. 2012) and a smaller seasonal cycle of surface heat fluxes upward to the atmosphere, and (2) the moistening of the atmosphere (Held and Soden 2006) leading to an enhanced seasonal cycle shortwave atmospheric absorption because water vapor is a strong shortwave absorber (Arking 1996) and the largest increases in shortwave absorption occur in the summer (when insolation is the greatest). Predicting how the seasonal cycle of atmospheric temperature will respond to global warming hinges critically on understanding how the seasonal heating of the atmosphere will change.

In this paper, we analyze the seasonal heating of the atmosphere in observations and in an ensemble of state of the art coupled climate models. We use observations and models in conjunction because the surface heat fluxes are poorly constrained in the observations and the similarities of the results in the observations and models demonstrate that the conclusions we reach are a consequence of the fundamental physics in both nature and the models, and not due to the uncertainty in the observational fluxes. This paper is organized as follows. In Section 2 we describe the data sets and models used and the basic method of analysis we will use throughout this study. In Section 3 we partition the zonal average seasonal heating of the atmosphere into shortwave atmospheric absorption and upward surface heat fluxes. We also analyze the spatial structure of the seasonal amplitude of atmospheric temperature. In Section 4, we trace the seasonal flow of energy through the climate system. We then analyze the seasonal cycle of energy fluxes averaged over the extratropical regions of each hemisphere and quantify seasonal energy fluxes between the ocean domain and the land domain. In Section 5 we analyze the change in the seasonal cycle due to a doubling of CO_2 in an ensemble of coupled climate models. A summary and discussion follows in Section 6.

2. Methods and datasets

a. Methods

The vertically integrated atmospheric energy budget is expressed as :

$$\frac{1}{g}\int_0^{P_S} \frac{\partial\left(c_P T + Lq\right)}{\partial t} dP = SWABS + SHF - OLR - \frac{1}{g}\int_0^{P_S} \left(\vec{U}\ \cdot \nabla E + \tilde{E}\ \nabla \cdot \vec{U}\right) dP \quad (1)$$

where P is the pressure (P_S is the surface pressure), E is moist static energy, OLR is the outgoing longwave radiation at the top of the atmosphere (TOA), and the term on the far right is the atmospheric energy flux divergence in advective form; $\vec{U}$ is the horizontal velocity, and g is the acceleration of gravity. The symbol ($\tilde{}$) represents the departure from the vertical average and the integration represents the mass integral over the atmospheric column. The advective form of the vertically integrated energy flux divergence is derived and discussed in the Appendix. $SWABS$ is the shortwave absorption within the atmospheric column defined as:

$$SWABS = SW\downarrow_{TOA} - SW\uparrow_{TOA} + SW\uparrow_{SURF} - SW\downarrow_{SURF}, \tag{2}$$

and represents the direct heating of the atmosphere by the sun. SHF is the upward flux of energy from the surface to the atmosphere and is composed of sensible heat fluxes ($SENS$), latent heat fluxes (LH) and longwave fluxes (LW) from the surface and the atmosphere:

$$SHF = SENS\uparrow_{SURF} + LH\uparrow_{SURF} + LW\uparrow_{SURF} - LW\downarrow_{SURF} . \tag{3}$$

We emphasize that SHF is defined as the energy exchange between the surface and the atmosphere and does not include the shortwave flux through the surface because the net shortwave flux at the surface represents an exchange of energy between the sun and the surface; it does not directly enter the atmospheric energy budget. A schematic of the energy exchange between the sun, atmosphere and, the surface is presented in Figure 1. Conceptually, the atmospheric energy tendency on the left hand side of Equation 1 is the difference between the atmospheric heating (by both surface fluxes – SHF – and by direct solar ab-

sorption within the atmosphere – $SWABS$) and the losses of energy from the atmospheric column (by the emission of outgoing longwave radiation and the atmospheric energy flux divergence).

We wish to analyze the role of the energy fluxes in amplifying/dissipating the seasonal cycle of temperature in the atmosphere. The magnitude of the seasonal cycle in temperature is quantified as the amplitude of the seasonal harmonic of temperature. The seasonal amplitude of the energy fluxes in Equation 1 is defined as the amplitude of the seasonal harmonic of the energy flux in phase with the solar insolation; this definition accounts for both the seasonal magnitude and phase of the energy fluxes with positive values amplifying the seasonal cycle of temperature in the atmosphere and negative values reducing the seasonal amplitude of temperature. The conclusions reached in the this manuscript do not depend on the choice of phase used to define the seasonal cycle. The same qualitative conclusions are reached if we define the seasonal amplitude using the phase of the atmospheric temperature or the total atmospheric heating ($SWABS$ + SHF).

b. Data sets and model output used

1) Observational data

The longwave and shortwave radiative fluxes at the TOA and the shortwave fluxes at the surface are from the Clouds and Earth's Radiant Energy System (CERES) experiment (Wielicki et al. 1996). We use the long term climatologies of the CERES TOA fluxes from Fasullo and Trenberth (2008a) that are corrected for missing data and global average energy imbalances. The surface shortwave radiation is taken from the CERES "AVG" fields that

159 are derived by assimilating the satellite observations into a radiative transfer model to infer
160 the surface radiative fluxes (Rutan et al. 2001). All calculations are preformed separately for
161 each of the four CERES instruments (FM1 and FM2 on Terra from 2000 -2005 and FM3 and
162 FM4 on AQUA from 2002 – 2005). We then average the results over the four instruments
163 to compose monthly averaged climatologies over the observation period.

164 The atmospheric heat flux divergences are calculated using the velocity, temperature,
165 specific humidity and geopotential fields from the ERA interim analysis. We use the 6 hourly
166 instantaneous fields with a horizontal resolution of 1.5° and 37 vertical levels to calculate the
167 atmospheric moist static energy fluxes using the advective form of the energy flux equations
168 (Trenberth and Smith 2008) as discussed in the Appendix. This method satisfies the mass
169 budget by construction and allows us to accurately calculate the energy flux divergences
170 without explicitly balancing the mass budget with a barotropic wind correction. We note
171 that, the calculated heat flux divergences are in close agreement with similar calculations by
172 Fasullo and Trenberth (2008b) and the conclusions reached in this study do not depend on
173 the dataset and methodology used to calculate the atmospheric energy fluxes. We calculate
174 the vertical integral of the atmospheric energy tendency as follows: (1) the temperature
175 and specific humidity tendency at each level is calculated as the centered finite difference of
176 the monthly mean fields and (2) the mass integral is calculated as the weighted sum of the
177 tendencies at each level multiplied by c_P and L respectively.

178 The *SHF* is calculated as the residual of the other terms in Equation 1, similar to
179 Trenberth (1997).

2) Model output

We use model output from the World Climate Research Programme's (WCRP) Coupled Model Intercomparison Project phase 3 (CMIP3) multi-model database (Meehl et al. 2007): a suite of standardized coupled simulations from 25 global climate models that were included in the International Panel on Climate Change's Fourth Assessment Report (https://esgcet.llnl.gov:8443/index.jsp). We use the pre-industrial (PI) simulations in which greenhouse gas concentrations, aerosols, and solar forcing are fixed at 1850 levels and the models are run forward for 400 years. We calculate model climatologies from the last 20 years of the PI simulations. The 16 coupled models that provided all the output fields that are required for the analysis presented in this study are listed in Table 1.

SWABS and *SHF* are calculated directly from the radiative and turbulent fluxes at the TOA and surface using Equations 2 and 3. The atmospheric column integrated energy tendency is calculated from the finite difference of the monthly mean vertical integral of the moist static energy. The atmospheric energy flux divergence is then calculated as the residual of Equation 1. We note that the method we use for calculating the *SHF* differs markedly between the models (where the surface energy fluxes are standard model output) and the observations (where surface energy fluxes are scarce and are diagnosed as a residual in this study).

3. Zonal average seasonal cycle of atmospheric heating

Figure 2 shows the observed seasonal variations of the zonally averaged *SWABS* and *SHF* with the annual average at each latitude removed. The seasonal cycle of *SWABS* is in phase with the solar insolation and has a seasonal amplitude of order 60 W m^{-2} in the extratropics. In the global and annual average, 21% of the incident shortwave radiation at the TOA is absorbed in the atmosphere (while 49% is absorbed at the surface and 30% is reflected back to space). The spatio-temporal structure of *SWABS* is predominantly (R^2 = 0.96) due to the spatio-temporal distribution of insolation; the spatial and seasonal variations in the shortwave absorptivity of the atmosphere make a very small contribution to the spatio-temporal distrubution of *SWABS* (i.e. *SWABS* is well approximated by assuming a spatial and temporal invariant fraction of the insolation is absorbed within the atmosphere). We find that, using the isotropic shortwave model of Donohoe and Battisti (2011), approximately 92% of *SWABS* (in the global average) is absorbed on the downward pass from the TOA to the surface and the enhancement of *SWABS* due to reflection of the Earth's surface is minimal. We note that Kato et al. (2011) recently demonstrated that CERES surface shortwave fluxes have uncertainities of order 10 W m^{-2} associated with uncertainities in the cloud and aerosol fields assimilated into the radiation model used to derive the fields. Projecting these errors onto the seasonal cycle of *SWABS* requires knowledge of the spatio-temporal structure of those uncertainities that are unknown and beyond the scope of this work. If the errors in CERES surface shortwave fluxes are zonally uniform and project perfectly onto the annual cycle (worse case scenario) the seasonal anomalies in *SWABS* derived here have uncertainities of order 20%. If the errors are random in space and time,

the errors in the seasonal anomalies in *SWABS* are less than 1%.

The seasonal variations of *SHF* are substantially smaller than the seasonal variations in *SWABS*. Over the southern ocean (between 30°S and 70°S) the seasonal variation in *SHF* oppose the seasonal heating of the atmosphere. In contrast, over the latitudes that have a substantial land fraction (between 45°N and 70°N and poleward of 70°S) the seasonal variations in *SHF* are in phase with the insolation. We understand these results as follows. The land surface is nearly in energetic equilibrium in the annual cycle due to the small heat capacity of the land surface (Fasullo and Trenberth 2008b), and so in these regions the seasonal variations in shortwave radiation at the surface are balanced by upwards *SHF* fluxes to the atmosphere. In contrast, the large heat capacity of the ocean allows the seasonal variations in shortwave radiation at the surface to be stored within the ocean mixed layer and the seasonal variations in surface shortwave radiation are not fluxed to the atmosphere. In fact, the ocean stores more energy seasonally than it absorbs directly from the sun (by as much as 30% in the latitude band of the Southern ocean) due to a net flux of energy from the atmosphere to the ocean (*SHF*) during the warm season.

We quantify the contribution of *SWABS* and *SHF* to the seasonal heating of the atmosphere as the amplitude of the annual Fourier harmonic in phase with the local insolation (see Section 2a for a discussion). This definition takes into account both the amplitude and phase of the annual cycle of energy fluxes with positive flux amplitudes amplifying the seasonal heating of the atmosphere and negative flux amplitudes reducing the seasonal heating of the atmosphere. We point the reader toward Figure 6 as a demonstration of how the total heating of the atmosphere is nearly in phase with the insolation and note that the same qualitative conclusions found here hold if we define the amplitude of the seasonal cycle from

the phase of the total heating or the phase of the column averaged atmospheric temperature. At all latitudes, the seasonal amplitude of *SWABS* is positive (*SWABS* is phase locked to the insolation) and exceeds that of *SHF* (solid lines in lower left panel of Figure 3). The seasonal amplitude of *SHF* is negative in the latitudes where ocean is prevalent and positive in the latitudes where land is prevalent. This result coincides with the seasonal phasing of *SHF* relative to the insolation noted over the same regions in Figure 2. We show in the bottom right panel of Figure 3 the fraction of atmospheric heating due to *SWABS*, defined as $|SWABS| \,/\, (|SWABS| + H(|SHF|))$ where $||$ brackets denote seasonal amplitudes and H is the Heaviside function. *SWABS* accounts for the vast majority of the seasonal atmospheric heating at all latitudes and all of the seasonal heating of the atmosphere in all latitude bands where ocean is prevalent.

The dominance of *SWABS* (relative to *SHF*) in the seasonal heating of the atmosphere is a stark contrast to the annual average atmospheric heating (top panels of Figure 3) where heating by *SHF* exceeds that by *SWABS* at all latitudes. In the global and annual average, the atmospheric heating is due to approximately two parts *SHF* and one part *SWABS* (see the top right panel of Figure 3). Conceptually, this result follows from the fact that, although the atmosphere is more transparent than absorbing resulting in more shortwave radiation reaching the surface than is absorbed within the atmosphere on all timescales, the annual average surface energy budget requires that the surface shortwave flux be balanced by *SHF* to the atmosphere. On shorter timescales, such as the seasonal cycle, no such balance is required: a significant fraction of the shortwave flux to the surface can be stored in the surface layer on shorter timescales.

SWABS and *SHF* from CMIP3 PI models are co-plotted with the observations in Figure

3 where the shading represents $\pm 1\sigma$ about the CMIP3 ensemble average. The observations and the models are in excellent agreement in all regions and seasons. The only significant difference between the models and observations is the annual the average *SHF* in the Arctic that is biased low in the models. Walsh et al. (2002) previously demonstrated that the downwelling surface fluxes are lower in the models than the observations in this region due to more clouds and optically thicker clouds than are observed and we believe this is the root cause of the bias. We emphasize that *SHF* is calculated as a residual from Equation 1 in the observations and directly from Equation 3 in the models; the correspondence of the relative contributions of *SWABS* and *SHF* to the seasonal and annual average atmospheric heating suggests that our conclusions are a consequence of fundamental physics in Nature and in the models and not due to methodology of our calculations or the observational field used here.

The source (*SHF* versus *SWABS*) of the seasonal heating of the atmosphere manifests itself in the spatial structure of the seasonal amplitude of temperature: observations are shown in Figure 4. *SHF*s primarily heat the lower troposphere whereas atmospheric heating by *SWABS* is nearly barotropic throughout the troposphere as can be seen in the left panel of Figure 4 which shows the vertical distribution of the seasonal amplitude of *SWABS* averaged poleward of 40° from a GFDL2.1 simulation of the pre-industrial climate[1]. The nearly barotropic profile of shortwave absorption in the troposphere is consistent with the profile of water vapor absorption (Chou and Lee 1996) whereas the isolated maximum in the stratosphere is due to ozone. In the latitude bands in which land is prevalent (poleward of 45°N and 70°S), the seasonal amplitude of *SHF* is positive (see Figure 3) and the seasonal amplitude of temperature is surface amplified. In the latitude bands where ocean is prevalent (30°N

[1]The shortwave atmospheric heating is not readily available in the CMIP3 archive.

to 40°N and 30°S to 70°S) and *SWABS* dominates the seasonal heating and the seasonal amplitude of temperature is nearly barotropic in the troposphere. The seasonal amplitude of temperature in the CMIP3 models (not shown) have a qualitatively similar structure in the latitude-level plane as in the observations. The seasonal amplitude of temperature therefore reflects the spatial structure of the atmospheric heating, suggesting that the seasonal heating of the atmosphere is not well mixed through the atmospheric column (i.e. via convection). In summary, the seasonal heating of the atmosphere is predominantly due to *SWABS* and the vertical structure of the atmospheric response (the seasonal amplitude of temperature) reflects the dominant source of heating.

4. The seasonal cycle of energy fluxes

The source of the seasonal heating of the atmosphere was discussed in the previous section. We now ask: how does the atmosphere balance the energy input from *SWABS* and *SHF* over the seasonal cycle? We start by looking at the zonal average seasonal energy balance. We then analyze the seasonal energy balance averaged over the extratropics in each hemisphere (subsection a) and the contribution of atmospheric energy transport between land and ocean regions to the seasonal cycle energy budget (subsection b). Finally, we demonstrate that the the source of the seasonal heating has implications for the vertical structure of the seasonal temperature response within the different regions (subsection c).

The seasonal amplitude (defined again as the seasonal amplitude of the annual Fourier harmonic in phase with the insolation) of all the atmospheric energy fluxes in Equation 1 are shown in Figure 5 for both the observations (solid lines) and the CMIP3 models (shad-

ing). The models and observations are in excellent agreement and the bulk structure of the seasonal amplitude at different latitudes is robust across the suite of CMIP3 models. With the exception of the tropics, meridional heat transport, OLR, and the loss of energy to atmospheric storage (the negative atmospheric energy tendency) all have negative seasonal amplitudes and thus act to damp the seasonal input of energy into the atmosphere[2]. In general the seasonal heating of the atmosphere (by *SWABS* plus *SHF*) is balanced by (listed in order of decreasing importance): (A) reduced (meridional) heat transport convergence (MHT), (B) enhanced OLR and, (C) atmospheric energy storage. As the atmosphere accumulates energy seasonally and temperature increases (term C) it exports energy dynamically to adjacent regions (term A) and radiatively to space (term B) and we can think of these three terms of the response of the atmosphere to seasonal heating. Energetic constraints require that the combined response be equal in magnitude to the combined heating by *SHF* and *SWABS* and Figure 5 shows that the atmospheric response is largest in the regions where *SHF* amplifies the seasonal cycle. The relative magnitudes of the response terms (OLR vs. meridional heat transport convergence vs. tendency) have been discussed by Donohoe (2011) and Donohoe and Battisti (2012) where it was argued that meridional heat transport convergence is the most efficient mechanism for the atmosphere to export energy, followed by OLR and energy storage.

The seasonal amplitude of both OLR and meridional heat transport convergence in the

[2]On the equatorward side of heat transport maximum (between 25°N and 40°N) the meridional heat transport divergence is in phase with the seasonal insolation and the heat transport amplifies the seasonal cycle. This effect is non-local; more energy is exported to the high latitudes in the cold season leading to a cooling of the subtropical atmosphere in the cold season.

southern extratropics is muted (with the exception of Antarctica) compared to that in the northern extratropics. This result follows from the fact that both *SWABS* and *SHF* heat the atmosphere in the northern extratropics where as *SHF* reduces the seasonal heating of the atmosphere in the southern extratropics. The total seasonal input of energy to the atmosphere is reduced in the southern hemisphere compared with the northern hemisphere and thus the atmospheric response (OLR, heat transport, and energy tendency) is reduced which coincides with the nearly seasonal invariance of storm activity in the southern hemisphere (Trenberth 1991; Hoskins and Hodges 2005).

a. Seasonal energy fluxes averaged over the extratropics

The seasonal cycle of energy fluxes (with the annual average removed) averaged over the extratropics of each hemisphere (poleward of 42°) is shown in the top panels of Figure 6. The observations (solid lines) and CMIP3 ensemble (shading) are in excellent agreement in both the seasonal amplitude of the energy fluxes and the phasing of each term. *SWABS* is in phase with the insolation and has similar seasonal amplitudes in the two hemispheres. In the southern extratropics, *SHF* is out of phase with the insolation; the seasonal heating of the atmosphere is accomplished entirely by *SWABS* and a portion of the seasonal atmospheric heating by *SWABS* is transferred to the ocean via *SHF*. Therefore, the seasonal storage of the energy in the ocean *exceeds* the seasonal variations in shortwave radiation at the surface. In contrast, *SHF* is in phase with the insolation in the NH extratropics. As a consequence, the seasonal amplitude of both OLR and (meridional) heat transport convergence in the northern extratropics is enhanced relative to the seasonal cycle in the southern extratropics

as is the seasonal cycle of atmospheric temperature. The atmospheric energy tendency leads the insolation in both hemispheres. In the southern extratropics the phase lead is 54 days in the observations and 51 $\pm$ 5 days in the CMIP3 PI ensemble (ensemble average and standard deviation). In the northern extratropics, the energy tendency leads the insolation by 62 days in the observations and 61 $\pm$ 4 days in the CMIP3 ensemble. Stated otherwise, the column average atmospheric temperature– which is in quadrature phase with the energy tendency– lags the insolation by approximately 30 days in the northern extratropics and 40 days in the southern extratropics or approximately one tenth of the annual forcing period. This phase lag is consistent with a system that is sinusoidally forced and has a linear damping (due to OLR and MHT energy export) that is approximately an order of magnitude larger than the heat capacity times the angular frequency of seasonal forcing[3].

The contribution of the various energy fluxes to the seasonal heating of the extratropical atmosphere in each hemisphere is summarized in the bottom panels of Figure 6. The left column shows the seasonal amplitude of the fluxes that heat the atmosphere seasonally (have positive seasonal amplitudes), the middle column shows the fluxes that damp the seasonal cycle (have negative seasonal amplitudes) and, the right column shows the atmospheric energy tendency. By construction, the sum of the heating terms (height of the left column) is balanced by the sum of the middle and right column. The key difference between the two hemispheres is that *SHF* serves as a heating term in the northern extratropics and as a damping term in the southern extratropics. As a result, the seasonal cycle of atmospheric

[3]The temperature response (T) of a system that is forced at angular frequency f satisfies the equation $C\frac{dT}{dt} = -\lambda T + e^{ift}$ where C is the heat capacity and λ is the linear damping (OLR and heat transport convergence). The phase lag of the temperature response (relative to the forcing) is $atan(\frac{fC}{\lambda})$.

energy, MHT, and OLR is larger in the northern hemisphere than that in the southern hemisphere.

b. The contrast in seasonal atmospheric energy fluxes between the land and ocean domains

The contrast of the seasonal phasing of *SHF* in the northern and southern extratropics is best understood by subdividing the northern extratropics into land and ocean domains (Figure 7). We also divide the observed atmospheric heat transport divergence into meridional and zonal components. We note that, in the zonal averages that were presented above, the zonal heat transport divergence is zero (by the divergence theorem) and that the zonal heat transport approximates the exchange of energy between the ocean and land domains in the northern extratropics where the coastlines are primarily orientated North to South. Over the land domain, the seasonal amplitude of the *SHF* is larger than that of *SWABS* and is in phase with the insolation (upper right panel of Figure 7). We understand this result as follows. First, the heat capacity of the land surface is very small resulting in a surface that is nearly in energetic equilibruim with the seasonal variation in surface shortwave radiation. Hence, the upward *SHF*s are in phase with the insolation. Second, the atmosphere is more transparent than absorbing for all seasons resulting in a seasonal amplitude of downwelling solar fluxes at the surface that exceeds *SWABS*. Therefore, the seasonal heating of the atmosphere over the land domain is dominated by surface energy fluxes as opposed to *SWABS*; this is shown in the lower right panel of Figure 7 and is very much akin to the annual average energy balance.

The phase of *SHF* over the land results in a large seasonal flux of energy to the atmosphere

that must be balanced by meridional and zonal energy exports, OLR, and atmospheric storage. Zonal energy fluxes (the dashed black lines in the upper panels of Figure 7) are the dominant mechanism of energy export. The zonal export of energy from the land to the ocean in the summer (and vice versa in the winter) is primarily accomplished by advection of the land-ocean temperature contrast by the time averaged atmospheric flow (not shown). This result agrees with the conclusion of Donohoe (2011) that zonal heat export is the most efficient energy export process for the extratropical atmosphere over the land and ocean domains. (Seasonal variations in MHT also contribute to energy export but the difference in the seasonal cycle of MHT over the land and the ocean domain is minimal; see the bottom panel of Figure 7). The zonal heat export into the ocean domain is equal and opposite that to the land domain and thus tends to amplify the seasonal cycle of the atmospheric temperature and energy fluxes over the ocean domain. This dynamical import of energy to the atmosphere above the ocean domain during the warm season is balanced primarily by energy export to the ocean via *SHF*. We emphasize that the seasonal energy storage in the northern ocean exceeds the seasonal variations in absorbed shortwave radiation at the surface which is a consequence of the zonal atmospheric heat import that ultimately is derived from shortwave heating of the land surface. As a hypothetical illustrative example, if the zonal flow of the atmosphere suddenly ceased in the middle of the summer, the atmosphere over the oceans would start cooling because the seasonal heating by $SWABS$ is completely removed by *SHF* (c.f. the height of the red and blue bars in the lower left panel of Figure 7). Similarly, in the winter, the ocean provides a source of heating (via *SHF*) that is nearly identical in magnitude to the atmospheric heating by the summer sun (via $SWABS$). The energy flux from the ocean to the atmosphere during the winter attenuates the seasonal

cycle of atmospheric temperatures over the land via the zonal atmospheric energy import. The portion of shortwave radiation incident on the land surface during the summer that gets stored in the ocean is returned to the land domain and warms the atmosphere above the land (relative to the purely radiative case) in the winter. The zonal atmospheric energy transport between the ocean and the land in the northern extratropics has a seasonal amplitude of 4.1 PW and is of comparable magnitude to the annual mean meridional heat transport in the atmosphere (Fasullo and Trenberth 2008a).

c. The seasonal temperature response by region

The seasonal input of energy into the atmosphere differs markedly between the ocean domain where the input is entirely by *SWABS* with a nearly vertically invariant heating profile throughout the troposphere (see left panel of Figure 4) and the land domain where *SHF* makes a substantial contribution to the lower atmosphere only. The source of seasonal heating is clearly reflected in the vertical structure of the seasonal amplitude of temperature averaged over the land and ocean domains of the northern hemisphere, shown in Figure 8. Over the northern land domain, the seasonal amplitude of temperature is surface amplified (reflecting the role of *SHF*) whereas over the northern ocean domain the seasonal amplitude is nearly barotropic to the tropopause (consistent with the profile of *SWABS*). Averaged over the whole of the northern extratropics, the seasonal amplitude of temperature is slightly surface amplified. The seasonal cycle of temperature averaged over the southern extratropics is nearly barotropic, consistent with the vertical heating profile of *SWABS* only over the southern ocean. The similarity of the vertical profile of seasonal heating and the seasonal

temperature response in each region suggests that the troposphere is not well mixed (by vertical turbulent energy fluxes) in the annual cycle; heating at a given vertical level results in a response localized in the vertical. The input of seasonal energy at the surface over land and it's subsequent removal at the surface over the ocean (see Subsection b) begs the question: at what vertical level does the zonal heat transport occur and how does the vertical structure of the temperature response reflect the vertical structure of the (zonal) heat transport? Further investigation is under way.

5. The response of the seasonal cycle of the atmosphere to CO_2 doubling

We now analyze the impact of the doubling of carbon dioxide on the seasonal heating of the atmosphere by *SWABS* and *SHF* and on the seasonal cycle of temperature. We have two expectations: First, as the globally averaged temperature increases the atmosphere will moisten (Held and Soden 2006) and the percent of incident shortwave insolation that is absorbed in the atmosphere will increase because water vapor is a strong absorber of shortwave radiation (Arking 1996; Chou and Lee 1996). The increase in *SWABS* will be greatest in the summer when the insolation is strongest, resulting in an increase in the amplitude of *SWABS*. Second, the melting of sea ice in the high-latitudes will expose ocean that was previously insulated from seasonal heat uptake. This is akin to replacing land with ocean and will result in a reduction of the seasonal amplitude of *SHF* and thus cause less net seasonal heating of the lower troposphere where ice melts.

a. Model runs used

We analyze output from the 1% CO_2 increase to doubling experiments in the CMIP3 archive (Meehl et al. 2007). The initial conditions for each model come from the equilibrated pre-industrial (PI) or in some cases (CCSM, MRI, and ECHAM) the present day (PD) simulations. Atmospheric CO_2 is increased by 1% per year until CO_2 has doubled relative to the PI concentration at 70 years. The simulations are then run forward for an additional 150 years with carbon dioxide fixed at twice the PI concentration. We average the model output over the last 20 years of these simulations (years 201-220 after CO_2 has started to ramp up) and compare the climatological fields to their counterparts in that model's PI (or PD) simulations. The 11 models that provided the necessary output fields used in this section are indicated with a 'yes' in the last column of Table 1. Hereafter, we will refer to these runs as the $2XCO_2$ runs.

b. Changes in the seasonal heating of the atmosphere due to CO_2 doubling

Figure 9 shows the CMIP3 ensemble average difference in the seasonal amplitude of atmospheric heating by *SWABS* and *SHF* between the $2XCO_2$ and the PI (or PD) runs. The ensemble average seasonal amplitude of *SWABS* increases by of order 2 W m^{-2} in the extratropics due to CO_2 doubling. This change is very robust across models in the extratropics (1σ about the ensemble average is given by the red shaded error in Figure 9 and is positive throughout the extratropics). Averaged over all the models, the fraction of incident shortwave radiation that is absorbed in the atmosphere increases by 0.8% in the annual and global average, from 22.4% in the PI simulations to 23.2% in the $2XCO_2$ runs. The change in

475 the seasonal amplitude of *SWABS*, in turn, is consistent with the seasonal amplitude of the
476 insolation at each latitude multiplied by the (0.8%) global and annual average increase in the
477 atmospheric absorptivity (not shown). We use the atmospheric radiative kernels of Previdi
478 (2010) to diagnose the contribution of water vapor shortwave absorption to the change in the
479 seasonal amplitude of *SWABS*. The product of the kernel and the water vapor change due
480 to CO_2 doubling in each CMIP3 model gives the change in atmospheric shortwave heating
481 due to the change in water vapor. The ensemble average change in the seasonal amplitude
482 of that quantity is shown by the dashed red line in Figure 9. Water vapor changes account
483 for almost all of the change in the seasonal amplitude of *SWABS* with the exception of the
484 high latitude of the southern ocean where we suspect changes in ozone may also contribute.
485 We note that the change in *SWABS* in the CMIP models due to CO_2 doubling are almost
486 enirely in the clear sky radiative fields (not shown) suggesting that clouds play a minnimal
487 role in the *SWABS* changes.

488 To examine the change in the vertical structure of the seasonal heating by *SWABS* due
489 to CO_2 doubling, we show in the left panel of Figure 10 the change (relative to the PI
490 simulation) in the seasonal amplitude of atmospheric shortwave heating averaged poleward
491 of 42° in the GFDL 2.1 simulation[4]. The enhanced *SWABS* heating in a moister atmosphere
492 (i.e. in the $2XCO_2$ world) is primarily in the upper troposphere where the fractional changes

[4]We did not analyze the change in the vertical distribution of shortwave radiative heating in the other CMIP3 models because these fields are not available in the CMIP3 archive. Given the robust nature of the humidity response to increasing CO_2 however, we anticipate that the change in the vertical structure of shortwave atmospheric heating in the other CMIP3 models will be similar to that shown in the left panel of Figure 10.

in water vapor due to CO_2 doubling are largest (not shown). Although the absolute change in specific humidity is smaller in the upper troposphere than in the lower troposphere, the downwelling radiation in the lower troposphere is depleted at the frequencies of shortwave water vapor absorption relative to downwelling radiation in the upper troposphere. As a result, the relatively small changes in specific humidity in the upper troposphere have a large local heating effect but a relatively small impact on the column integrated *SWABS*; it essentially redistributes the shortwave heating from the lower troposphere to the upper troposphere. Integrated over the atmospheric column, shortwave absorption is enhanced by $2\mathrm{Wm}^{-2}$ due to more absorption in the wings of water vapor absorption bands in the moister atmospheric column. As a consequence, the seasonal heating of the atmosphere by *SWABS* is enhanced in a warmer world and more so in the upper troposphere than in the lower troposphere.

The most pronounced (and robust across models) change in the seasonal heating of the atmosphere due to CO_2 doubling is the reduced seasonal amplitude of *SHF* poleward of 60° in both hemispheres (the solid blue line in Figure 9). The vast majority of this change occurs within the sub-domain where sea ice melts, as shown in Figure 9. This result can be understood as follows. Sea ice insulates the ocean from the exchange of energy with the atmosphere (Serreze et al. 2007) so the effective surface heat capacity of a region with extensive sea ice is much smaller than that of an open ocean (i.e. the heat capacity of the ocean mixed layer). As a consequence, the contributions to the seasonal heating of the atmosphere above regions that are covered with sea ice is similar to that above land regions: seasonal variations in *SHF* to the atmosphere amplify the seasonal heating due to *SWABS* (as in the upper right hand panel of Figure 7). Melting the sea ice exposes the atmosphere

to the higher heat capacity of the open ocean so seasonal variations in shortwave radiation at the surface over these regions are now balanced by ocean heat storage as opposed to the upward energy fluxes (*SHF*). Hence, the seasonal flow of energy is now from the atmosphere to the ocean during the summer (as in the upper left panel of Figure 7). Thus the seasonal amplitude of *SHF* decreases as the ice melts and more of the atmosphere is exposed to the (high heat capacity) ocean mixed layer as was demonstrated by (Dwyer et al. 2012).

The seasonal amplitude of *SHF* increases between 45° and 60° in both hemispheres due to CO_2 doubling. In the northern hemisphere, this is largely due to an increase (relative to the PI simulation) in the seasonal amplitude of downwelling shortwave radiation at the land surface (not shown) resulting in larger seasonal variations in *SHF*, as required by the surface energy budget given the small heat capacity of the land surface. This process accounts for the vast majority of the increases in the seasonal amplitude of *SHF* in the midlatitudes of the northern hemisphere (not shown) but it does not explain the increased seasonal amplitude of *SHF* in the midlatitudes of the southern hemisphere. The cause of the enhanced seasonal amplitude of *SHF* between 50°S and 60°S is under further investigation.

c. Changes in the seasonal amplitude of temperature due to CO_2 doubling

The spatial structure of the change in the seasonal amplitude of temperature due to CO_2 doubling reflects the change in atmospheric heating induced by a moistening of the atmosphere and the melting of sea ice in the high latitudes. As shown in section 5b, doubling CO_2 causes a robust increase in the seasonal shortwave heating in the upper troposphere throughout the extratropics and a robust decrease in the seasonal heating of the atmosphere

by surface fluxes poleward of 60° in both hemispheres. These changes in the seasonal heating of the atmosphere have a clear and robust imprint on the change in the seasonal amplitude of temperature relative to the PI simulations (right panel of Figure 10). The seasonal amplitude of temperature decreases in the lower atmosphere where the seasonal amplitude of *SHF* is reduced in a $2XCO_2$ world. In contrast, the seasonal amplitude of temperature is enhanced in the upper troposphere of the extratropics in a $2XCO_2$ world where the seasonal amplitude of shortwave heating is enhanced. The vertical profile of the change in the amplitude of the seasonal cycle of temperature matches that of the shortwave absorption. The vertical structure of the seasonal temperature response to CO_2 doubling is robust across models, as assessed by a one sample t-test of the change due to CO_2 doubling in each model at the 99% confidence interval (the regions enclosed by the red and blue dashed contours in Figure 10 are significantly different from zero).

At 30° in each hemisphere, the seasonal amplitude of the near surface temperature is enhanced in the $2XCO_2$ simulations despite the reduction in the seasonal amplitude of *SHF*. This behavior is a consequence of a deepening of the subtropical boundary layer in the warmer planet and the climatological phasing of *SHF* in this region which opposes the dominant solar heating (see Figure 5). The surface damping of the seasonal cycle by *SHF* over a deeper layer results in an enhanced seasonal cycle of temperature at the surface in the $2XCO_2$ world. The cause of the deepened boundary layer is beyond the scope of this work but we speculate that a reduction of subsidence associated with the weakening (Tanaka et al. 2005) and widening (Seager and Coauthors 2007) of the Hadley circulation is the root cause.

6. Summary and discussion

The seasonal cycle of atmospheric temperature has large socioeconomic and ecological impacts. Both the amplitude and phase of the seasonal cycle are projected to change due to global warming (Mann and Park 1996) and trends in the seasonal cycle have been observed over the last century (Stine et al. 2009; Thomson 1995). Understanding the source of the seasonal heating of the atmosphere is critical to understanding the projected change in the seasonal cycle of temperature in the atmosphere.

The seasonal heating of the atmosphere differs markedly from the annual average atmospheric heating. While the annual average heating is dominated by upward energy fluxes from the surface, the vast majority of the seasonal heating is due to shortwave absorption within the the atmosphere that is nearly vertically invariant throughout the troposphere. The annual average surface energy budget requires that the net shortwave flux at the surface be balanced by an upward energy flux to the atmosphere. The same constraint does not apply to the annual cycle where shortwave surface heating can be balanced by surface energy storage. Thus, although the atmosphere is more shortwave transparent than shortwave absorbing, our results show that the seasonal heating of the atmosphere is dominated by shortwave atmospheric heating because the shortwave absorption is considerable and the insolation that is transmitted to the surface primarily goes into storage (especially over the ocean). In fact, across most of the planet, the atmosphere is seasonally heated by directly absorbing energy from the sun (by $SWABS$) during the summer and subsequently fluxes a portion of this energy to the ocean. In contrast to the annual average, over the seasonal cycle the atmosphere is heated from above and is cooled slightly from below (the global average

seasonal amplitude of *SHF* is slightly negative).

The limited heat capacity of the land surface requires that seasonal variations in surface solar radiation over the land domain are primarily balanced by upward energy fluxes to the atmosphere so that the heating of the atmosphere over the seasonal cycle is primarily by upward surface energy fluxes (*SHF*) and secondarily by atmospheric shortwave absorption (*SWABS*), as can be seen in the lower right panel of Figure 7. In the midlatitudes of the NH, the gross differences in the seasonal atmospheric heating over the land domain and the ocean domain forces a seasonally varying zonal energy exchange between the land and ocean domain of 4.1 PW which is comparable in magnitude to the annually averaged atmospheric meridional heat transport in each hemisphere. The vertical structure of the seasonal amplitude of atmospheric temperature clearly reflects the different contribution of *SWABS* and *SHF* to the net seasonal heating over the land and ocean domains. Where ocean is prominent and seasonal heating by *SWABS* is dominant, the seasonal amplitude of temperature is nearly barotropic throughout the troposphere and coincides with the vertical structure of *SWABS*. In contrast, over the land domain the seasonal amplitude of temperature is surface amplified, reflecting the contribution of upward energy fluxes from the surface (*SHF*) to the seasonal heating.

The change in the seasonal heating of the atmosphere due to CO_2 doubling is a consequence of two different physical processes that are robust across the CMIP3 ensemble (Figure 9) and have a clear physical interpretation: First, enhanced CO_2 causes a moistening of the atmosphere which, in turn, causes more shortwave absorption in the troposphere–particularly in the upper troposphere (see the left panel of Figure 10). These effects are most pronounced in the summer, when the insolation is the greatest, leading to an enhanced

seasonal cycle of heating in a warmer world. Second, enhanced CO_2 causes a reduction in the area covered by sea ice, which results in more of the seasonal variations in solar insolation being transmitted to the (large heat capacity) ocean. Thus the seasonal heating of the atmosphere by upward surface energy fluxes (*SHF*) is reduced in the high latitudes in a $2XCO_2$ world. The change in the seasonal heating of the atmosphere due to CO_2 doubling has a clear imprint on the seasonal amplitude of atmospheric temperature; the seasonal cycle of temperature increases in the upper troposphere of the extratropics (where the seasonal amplitude of *SWABS* increases) and decreases at the surface in the polar regions (where the seasonal amplitude of *SHF* decreases) due to CO_2 doubling (Figure 10). As a consequence, the atmospheric column in a $2XCO_2$ world is stabilized in the summer and destabilized in the winter.

In our study, we have formulated the atmospheric energy budget in terms of the shortwave energy absorbed within the atmosphere and the net (non-solar) exchange of energy between the surface and the atmosphere. Our approach differs from the traditional approach of Fasullo and Trenberth (2008a) that views the atmospheric energy budget in terms of the difference between the total energy flux into the top of the atmosphere and the surface. The traditional viewpoint emphasizes the near seasonal balance of insolation at the TOA and the energy flux (solar included) to the surface; by and large, the oceans are seasonally heated by the sun. The traditional approach is less useful for understanding the source of the seasonal heating of the atmosphere (where the seasonal heating of the atmosphere is the residual of the TOA and surface fluxes). Our formulation illuminates the relative importance of atmospheric shortwave absorption and surface energy fluxes for the seasonal cycle of temperature in the troposphere.

Our work demonstrates that the atmospheric response to heating is localized in the vertical and further suggests that the net radiative forcing at the tropopause (i.e. the Solomon et al. 2007, definition of radiative forcing) is not a useful concept on short timescales because it fails to distinguish between energy absorbed within the atmospheric column and energy absorbed at the surface. The vertical structure of atmospheric heating within the troposphere is irrelevant provided the surface layer is in energetic equilibrium and the troposphere is well mixed in the vertical. Our results demonstrate that neither of these conditions are satisfied in either the climatological or perturbed ($2XCO_2$) seasonal cycles and the atmospheric temperature response depends critically on the vertical distribution of the heating. This work begs the question: on what timescales and regimes is the radiative forcing at the tropopause a useful concept and when is the response of the system contingent on the vertical structure of the atmospheric forcing? We hope to explore the impact of the vertical structure of atmospheric forcing on the atmospheric temperature response across a myriad of spatio-temporal scales in future work.

APPENDIX

Derivation of the atmospheric energy budget equation

The vertically integrated atmospheric energy budget equation is developed, starting from the the dry energy and moisture equations of Trenberth and Smith (2008) at a given vertical level (their Equations 3a and 5). Multiplying the moisture equation by L, adding it to the dry energy equation and vertically integrating over pressure levels from the TOA to the surface (P_S) gives:

$$\frac{1}{g}\int_0^{P_S}\frac{\partial}{\partial t}\left(c_P T + K + Lq\right)dP + \frac{1}{g}\int_0^{P_S}\vec{U}\cdot\nabla\left(E+K\right)dP + \frac{1}{g}\int_0^{P_S}\omega\frac{\partial}{\partial P}\left(E+K\right)dP = SWABS + SHF - OLR, \tag{A1}$$

where E is the moist static energy, K is the kinetic energy, ω is the pressure velocity and the vertically integrated diabatic heating (Q1-QF) have been reorganized into the terms used in this study. The first term is the energy tendency in the atmospheric column. The second term is the horizontal advection of energy. The third term represents the vertical advection of energy and is primarily associated with subsidence warming in regions of net descent and adiabatic cooling in regions of net ascent. The right hand side of the equation is the net heating of the atmospheric by radiative and diabatic processes.

We can rewrite the vertical advection term (third term on the right) by first integrating

by parts and then invoking the Boussinesq approximation:

$$\begin{aligned} &\frac{1}{g}\int_0^{P_S} \omega \frac{\partial}{\partial P}\left(E+K\right) dP \\ &= \frac{1}{g}\left[\left(E+K\right)\omega\right]\Big|_0^{P_S} - \frac{1}{g}\int_0^{P_S}\left(\left[E+K\right]\frac{\partial \omega}{\partial P}\right) dP \\ &= \frac{1}{g}\left(E_S+K_S\right)\frac{\partial P_S}{\partial t} + \int_0^{P_S}\left(E+K\right)\nabla\cdot\vec{U} dP \end{aligned} \qquad \text{(A2)}$$

where E_S and K_S are the moist static and kinetic energy at the surface. If we subdivide the E into the vertical average, [E], and an anomaly from the vertical average, $\tilde{E}$ we can make one additional simplification and gain insight into the physical interpretation of equation A2:

$$\begin{aligned} &\frac{1}{g}\int_0^{P_S} \omega \frac{\partial}{\partial P}\left(E+K\right) dP \\ &\quad = \frac{1}{g}\left(E_S+K_S\right)\frac{\partial P_S}{\partial t} + \frac{\left[E+K\right]}{g}\int_0^{P_S}\nabla\cdot\vec{U} dP + \frac{1}{g}\int_0^{P_S}\left(\tilde{E}+\tilde{K}\right)\nabla\cdot\vec{U} dP \end{aligned} \qquad \text{(A3)}$$

If the mass of the atmospheric column is conserved, both the surface pressure tendency and the vertical integral of the divergence will be zero and only the third term on the right of equation A3 remains. This term says that energy is input into the column (the energy flux divergence on the LHS is negative) when there is convergence at levels of relatively high E ($\tilde{E} > 0$) and divergence at levels of relatively low E ($\tilde{E} < 0$). Since E increases with height in the atmosphere (with the exception of the boundary layer), this statement says that the column gains energy when there is convergence aloft and divergence at the surface as is the case on the poleward side of the thermally direct Hadley cell (the subtropics) where the vertical structure of horizontal divergence forces large scale subsidence warming. If the mass of the column is not conserved, then mass balance requires that

$$\frac{1}{g}\int_0^{P_S} \nabla \cdot \vec{U} dP = -\frac{1}{g}\frac{\partial P_S}{\partial t}. \tag{A4}$$

(In equation A4, we have ignored the mass source associated with evaporation minus precipitation which is two orders of magnitude smaller than the other terms (Trenberth 1997)). Substituting Equation A4 into equation A3 results in the near cancellation of the first two terms; the two terms differ by the energy contrast between the surface and the column average energy. Using $\tilde{tilde}$ to represent the anomaly from the vertical average gives

$$\frac{1}{g}\int_0^{P_S} \omega \frac{\partial}{\partial P}\left(E + K\right) dP$$
$$= \frac{1}{g}\left(\tilde{E_S} + \tilde{K_S}\right)\frac{\partial P_S}{\partial t} + \frac{1}{g}\int_0^{P_S}\left(\tilde{E} + \tilde{K}\right)\nabla \cdot \vec{U} dP \quad . \tag{A5}$$

The magnitude of $\left(\tilde{E_S} + \tilde{K_S}\right)$ in the first term is comparable to that of the magnitude of $\tilde{E}$ in the integrand of the second term. $\tilde{E}$ increases with pressure and crosses zero in the mid-troposphere. $\nabla \cdot \vec{U}$ also has a simple vertical structure with divergence aloft and convergence at the surface (e.g. in the upper and lower branches of the Hadley cell) or vice versa. Therefore, the magnitude of the second term in equation A5 is of order the product of the average magnitude of $\nabla \cdot \vec{U}$ and $\tilde{E}$. Integrated over the column as a whole, the layers of convergence and divergence nearly balance each other out; the average magnitude of the divergence exceeds the column average divergence by two orders of magnitude (not shown). Because $\frac{\partial P_S}{\partial t}$ is equal to the column average divergence (by equation A4), the first term on the RHS in equation A5 is approximately two orders of magnitude smaller than the second term, and we thus neglect the first term in this study. The impact of ignoring this term on the calculations performed in this manuscript is shown in Figure 11 and is small.

In our calculations, we also ignore kinetic energy which is two orders of magnitude smaller than the moist static energy. We assess the magnitude of the kinetic energy's contribution to the seasonal amplitude of energy fluxes in the following manner: (1) the climatological energy flux divergence and total column energy tendency of Trenberth and Stepaniak (2003) are used as a starting point, (2) the kinetic energy contribution is subtracted from the total energy flux divergence and tendency (3) the seasonal amplitude of these fields is calculated as the annual harmonic of the zonal mean energy flux in phase with the insolation. The seasonal amplitude of these fields including and excluding the kinetic energy is shown in Figure 12. We emphasis that the inclusion of kinetic energy makes a small contribution to the calculations presented in this manuscript. Excluding kinetic energy from the equation, the atmospheric energy budget equation becomes

$$\frac{1}{g}\int_0^{P_S} \frac{\partial\left(c_P T + LQ\right)}{\partial t} dP = SWABS + SHF - OLR - \frac{1}{g}\int_0^{P_S} \left(\vec{U}\ \cdot \nabla E + \tilde{E}\ \nabla \cdot \vec{U}\right) dP, \tag{A6}$$

which is equation 1 of this paper.

We emphasize that the differences between the flux form methodology of calculating energy fluxes used by Fasullo and Trenberth (2008a) and Trenberth and Stepaniak (2003) and the advective form of the energy fluxes used here (compare Figures 12 and 5) are very small and do not affect the conclusions found in this manuscript. The advantages of this form of the equation over the more commonly used flux form (Trenberth and Stepaniak 2003) are that (A) the decomposition of the heat flux divergence into advective and divergent components lends insight into the processes that contribute to the accumulation of energy

in the column, (B) the heat flux calculations can be done without explicitly balancing the mass budget with a barotropic wind correction and (C) the energy budget is invariant to the zero point energy.

Acknowledgments.

ECMWF ERA-40 data used in this study/project have been provided by ECMWF/have been obtained from the ECMWF Data Server. This work was supported by the NOAA Global Change Postdoctoral Fellowship. We thank Dargan Frierson for providing the GFDL shortwave heating fields and Michael Previdi for the use of his radiative kernels.

REFERENCES

Arking, A., 1996: Absorption of solar energy in the atmosphere: Discrepancy between model and observations. *Science*, **273**, 779.

Chou, M. and K. Lee, 1996: Parameterizations for the absorption of solar radiation by water vapor and ozone. *J. Atmos. Sci.*, **53**, 1203–1208.

Dines, W. H., 1917: The heat balance of the atmosphere. **43**, 151–158.

Donohoe, A., 2011: Radiative and dynamic controls of global scale energy fluxes. Ph.D. thesis, University of Washington, 137 pp.

726 Donohoe, A. and D. Battisti, 2011: Atmospheric and surface contributions to planetary
727 albedo. *J. Climate*, **24 (16)**, 4401–4417.

728 Donohoe, A. and D. Battisti, 2012: What determines meridional heat transport in climate
729 models? *J. Climate*, **25**, 3832–3850.

730 Dwyer, J., M. Biasutti, and A. Sobel, 2012: Projected changes in the seasonal cycle of surface
731 temperature. *J. Climate*, **25**, 6359–6374.

732 Fasullo, J. T. and K. E. Trenberth, 2008a: The annual cycle of the energy budget: Part 1.
733 global mean and land-ocean exchanges. *J. Climate*, **21**, 2297–2312.

734 Fasullo, J. T. and K. E. Trenberth, 2008b: The annual cycle of the energy budget: Part 2.
735 meridional structures and poleward transports. *J. Climate*, **21**, 2313–2325.

736 Fels, S. B., 1985: Radiative-dynamical interactions in the middle atmosphere. *Adv. Geophys.*,
737 **28A**, 277–300.

738 Gupta, S., N. Ritchey, A. C. Wilber, and C. H. Whitlock, 1999: A climatology of surface
739 radiation budget derived from satellite data. *J. Climate*, **12**, 2691–2710.

740 Held, I., R. Hemler, and V. Ramaswamy, 1993: Radiativeconvective equilibrium with explicit
741 two-dimensional moist convection. *J. Atmos. Sci.*, **50**, 3909–3927.

742 Held, I. and B. Soden, 2006: Robust responses of the hydrological cycle to global warming.
743 *J. Appl. Meteor.*, **19 (21)**, 5686–5699.

744 Hoskins, B. J. and K. I. Hodges, 2005: A new perspective on southern hemisphere storm
745 tracks. *J. Climate*, **18**, 4108–4129.

746 Kato, S., et al., 2011: Improvements of top-of-atmosphere and surface irradiance computa-
747 tions with calipso-, cloudsat-, and modis-derived cloud and aerosol properties. *J. Geophys.*
748 *Res.*, **116**, doi:10.1029/2011JD016050.

749 Kiehl, J. and K. E. Trenberth, 1997: Earth's annual global mean energy budget. *Bull. Amer.*
750 *Meteor. Soc.*, **78**, 197–208.

751 Manabe, S. and T. Wetherald, 1967: Thermal equilibrium of the atmosphere with a given
752 distribution of specific humidity. *J. Atmos. Sci.*, **24**, 241–259.

753 Mann, M. and J. Park, 1996: Greenhouse warming and changes in the seasonal cycle of
754 temperature: Model versus observations. *Geophys. Res. Lett.*, **23**, 1111–1114.

755 Meehl, G. A., C. Covey, T. Delworth, M. Latif, B. McAvaney, J. F. B. Mitchell, R. J.
756 Stouffer, and K. E. Taylor, 2007: The WCRP CMIP3 multi-model dataset: A new era in
757 climate change research. *Bull. Amer. Meteor. Soc.*, **88**, 1383–1394.

758 Previdi, M., 2010: Radiative feedbacks on global precipitation. *Environ. Res. Lett.*, **5**, doi:
759 doi:10.1088/1748-9326/5/2/025211.

760 Rutan, D., F. Rose, N. Smith, and T. Charlock, 2001: Validation data set for CERES surface
761 and atmospheric radiation budget (SARB). *WCRP/GEWEX Newsletter*, **11 (1)**, 11–12.

762 Seager, R. and Coauthors, 2007: Model projections of an imminent transition to a more arid
763 climate in southwestern north america. *Science*, **316**, 1181–1184.

764 Serreze, M., A. Barrett, A. Slater, M. Steele, J. Zhang, and K. Trenberth, 2007: The large-
765 scale energy budget of the arctic. *J. Geophys. Res.*, **112**, doi:10.1029/2006JD008230.

766 Solomon, S., D. Qin, M. Manning, Z. Chen, M. Marquis, K. Averyt, M.Tignor, and H. Miller,
767 2007: *The scientific basis. Contribution of Working Group 1 to the Third Assessment*
768 *Report of the Intergovernmental Panel on Climate Change*. Cambridge University Press.

769 Stine, A., P. Huybers, and I. Fung, 2009: Changes in the phase of the annual cycle of surface
770 temperature. *Nature*, **457 (435- 440)**, 123–139.

771 Takahashi, K., 2009: The global hydrological cycle and atmospheric shortwave absorption
772 in climate models under CO_2 forcing. *J. Climate*, **22**, 5667–5675.

773 Tanaka, H. L., N. Ishizaki, and D. Nohara, 2005: Intercomparison of the intensities and
774 trends of hadley, walker and monsoon circulations in the global warming projections.
775 *SOLA*, **1**, 77–80.

776 Thomson, D., 1995: The seasons, global temperature, and precession. *Science*, **268**, 59–68.

777 Trenberth, K. E., 1991: Storm tracks in the southern hemisphere. *J. Atmos. Sci.*, **48**, 2159–
778 2178.

779 Trenberth, K. E., 1997: Using atmospheric budgets as a constraint on surface fluxes. *J.*
780 *Climate*, **10**, 2796–2809.

781 Trenberth, K. E., J. T. Fasullo, and J. Kiehl, 2009: Earth's global energy budget. *Bull.*
782 *Amer. Meteor. Soc.*, **90 (3)**, 311–324.

783 Trenberth, K. E. and L. Smith, 2008: Atmospheric energy budgets in the Japanese reanalysis:
784 Evaluation and variability. **86**, 579–592.

785 Trenberth, K. E. and D. P. Stepaniak, 2003: Co-variability of components of poleward
786 atmospheric energy transports on seasonal and interannual timescales. *J. Climate*, **16**,
787 3691–3705.

788 Trenberth, K. E. and D. P. Stepaniak, 2004: The flow of energy through the earth's climate
789 system. *Quart. J. Roy. Meteor. Soc.*, **130**, 2677–2701.

790 Walsh, J., V. Kattsov, W. Chapman, V. Govorkova, and T. Pavlova, 2002: Comparison
791 of arctic climate simulations by uncoupled and coupled global models. *J. Climate*, **15**,
792 1429–1446.

793 Wielicki, B., B. Barkstrom, E. Harrison, R. Lee, G. Smith, and J. Cooper, 1996: Clouds and
794 the earth's radiant energy system (CERES): An earth observing system experiment. *Bull.*
795 *Amer. Meteor. Soc.*, **77**, 853–868.

List of Tables

1 Models used in this study and their resolution. The horizontal resolution refers to the latitudinal and longitudinal grid-spacing or the spectral truncation. The vertical resolution is the number of vertical levels. The last column indicates if the model is included in the analysis of the $2XCO_2$ runs in Section 5. 42

Abbreviation	Full Name	Horizontal Resolution	Vertical Resolution	$2XCO_2$ run
BCCR-BCM2.0	Bjerknes Centre for Climate Research, University of Bergen, Norway	T63	L31	Yes
CCCMA-CGCM3.1	Canadian Centre for Climate Modeling and Analysis, Canada	T47	L31	Yes
CNRM-CM3	Meteo-France/Centre National de Recherches Meteorologique, France	T63	L45	Yes
CSIRO-MK3.0	Australian Commonwealth Scientific and Research Organization (CSIRO), Australia	T63	L18	Yes
GFDL-CM2.0	NOAA/Geophysical Fluid Dynamics Laboratory, USA	2.0° X 2.5°	L24	No
GFDL-CM2.1	NOAA/Geophysical Fluid Dynamics Laboratory, USA	2.0° X 2.5°	L24	Yes
IAP-FGOALS	National Key Laboratory of Numerical Modeling for Atmospheric Sciences and Geophysical Fluid Dynamics (LASG), China	T42	L26	No
MPI-ECHAM5	Max Planck Institute for Meteorology, Germany	T63	L31	No
INM-CM3.0	Institute for Numerical Mathematics, Russia	4° X 5°	L21	Yes
IPSL-CM4.0	Institute Pierre Simon Laplace, France	2.5° X 3.75°	L19	Yes
Micro3.2 (Medres)	National Institute for Environmental Studies, and Frontier Research Center for Global Change, Japan	T42	L20	No
Micro3.2 (Hires)	National Institute for Environmental Studies, and Frontier Research Center for Global Change, Japan	T106	L56	No
MRI-CGCM2.3.2a	Meteorological Research Institute, Japan	T42	L30	Yes
NCAR-CCSM3.0	National Center for Atmospheric Research, USA	T85	L26	Yes
UKMO-HADCM3	Hadley Centre for Climate Prediction and Research/Met Office, UK	2.5° X 3.8°	L19	Yes
MIUB-ECHOg	University of Bonn, Germany	T30	L19	Yes

TABLE 1. Models used in this study and their resolution. The horizontal resolution refers to the latitudinal and longitudinal grid-spacing or the spectral truncation. The vertical resolution is the number of vertical levels. The last column indicates if the model is included in the analysis of the $2XCO_2$ runs in Section 5.

List of Figures

1 Schematic of the energy exchanges between the sun, the atmosphere, and the surface. *SWABS* is the solar insolation absorbed within the atmosphere. *SHF* is the net upward energy flux from the surface to the atmosphere. *OLR* is the outgoing longwave radiation at the top of the atmosphere. The surface solar fluxe (dashed line) is the solar flux to the surface and does not enter the atmospheric energy budget because this radiation passes through the atmosphere. 48

2 Observed zonal mean seasonal cycle of atmospheric heating by atmospheric solar absorption (*SWABS* – top panel) and by upward surface heat fluxes (*SHF* – bottom panel) in W m^{-2}. The annual average at each latitude has been removed. The atmospheric solar absorption is calculated from the CERES data at the TOA and surface and the surface heating is calculated from the residual of the terms in Equation 1 as discussed in the text. 49

3 Zonal mean heating of the atmosphere in the annual average (top panel) and in the seasonal cycle (bottom panel). The heating is divided into atmospheric shortwave absorption (SWABS, red) and upward surface fluxes (blue). The right panels show the fractional contribution of SWABS to the total heating (defined as $SWABS$ / ($SWABS + H(SHF)$) where H is the Heaviside function and the tropics are excluded from the seasonal calculation. The seasonal amplitude is defined throughout as the amplitude of the Fourier harmonic in phase with the sun. In each figure, the solid line is the observations and the shading is $\pm 1\sigma$ about the ensemble mean pre-industrial simulations from the CMIP3 models. 50

4 (Left panel) The vertical distribution of the seasonal amplitude of $SWABS$ averaged over the extratropics from a pre-industrial simulation of the GFDL 2.1 model. (Right panel) The observed zonal mean seasonal amplitude of temperature. 51

5 The seasonal amplitude of atmospheric energy fluxes in phase with the sun (positive fluxes amplify the seasonal cycle, negative fluxes reduce the seasonal cycle). Solid lines are observations and shaded regions represent $\pm 1\sigma$ about the ensemble mean pre-industrial simulations from the CMIP3 models. 52

6 (top panel) The seasonal cycle of atmospheric energy fluxes(in W m^{-2}) averaged over the extratropics – defined as poleward of 42°– in the southern hemisphere (left panel) and the northern hemisphere (right panel). The observations are shown by the solid lines and the shaded region represents $\pm 1\sigma$ about the CMIP3 PI ensemble average. The dashed vertical lines represent the winter solstice in the SH plot and summer solstice in the NH plot. The annual average of each term has been removed. (bottom panel) The seasonal amplitude of the atmospheric energy fluxes in phase with the seasonal cycle of solar insolation averaged over the extratropics (the left panel is the southern extratropics and the right panel is the northern extratropics). The terms that amplify the seasonal cycle in temperature (heating) are in the first column. The seasonal energy loss terms (cooling) are in the second column. The third column is the energy stored in the atmospheric column (energy tendency). The individual terms are color coded in the legend in the upper left panel and explained in the text. 53

7 (top panels) The seasonal cycle of energy fluxes averaged over the atmosphere in the NH extratropical ocean domain (left panel) and land domain (right panel). Observations are given by solid lines and the shading represents 1 of the CMIP3 pre-industrial ensemble. The atmospheric heat fluxes are decomposed into zonal and meridional components in the observations. The vertical dashed line represents the summer solstice. (bottom panels) The seasonal amplitude of energy fluxes (in phase with the sun) averaged over the ocean/land domains. The amplifying fluxes are on the left and the damping (i.e, out of phase fluxes) are in the middle (colors are described in the legend). 54

8 The seasonal amplitude of temperature averaged over the extratropics (poleward of 42°) in each hemisphere (in K). The northern extratropics is further decomposed into ocean and land domains. The observations are given by the solid line and the shading represents $\pm 1\sigma$ about the ensemble mean pre-industrial simulations from the CMIP3 models. 55

9 The change in the seasonal amplitude of atmospheric heating in the CMIP3 CO_2 doubling experiment. The solid red line is the ensemble average change in *SWABS*, the shaded red area is $\pm 1\sigma$ of the model response and, the dotted red line is the change due to water vapor changes as diagnosed from the water vapor shortwave kernel. The blue line is the change in the seasonal amplitude of *SHF* (with shading $\pm 1\sigma$) and the dotted blue line is the change within the sub portion of the latitude band where the sea ice fraction decreases by more than 10% relative to the PI simulation. 56

10 (Right Panel) Zonal and ensemble average change in the seasonal amplitude of temperature in the CMIP3 CO_2 doubling experiments. The contours show the regions of significant change as assessed by a one sample t-test at the 99% confidence interval. (Left Panel) The vertical profile of the change in the seasonal amplitude of shortwave radiative heating in the GFDL 2.1 CO_2 doubling experiment expressed as the change in column integrated *SWABS* in W m^{-2} that would result if that heating rate were vertically invariant over the entire column. 57

11 Effect of neglecting the mass column tendency on the energy flux calculations presented in this manuscript. The solid line is the seasonal amplitude of the zonal average energy flux convergence using all terms and the dashed line is the same calculation neglecting the column mass tendency term (first term in Equation A5). 58

12 Effect of neglecting the kinetic energy on the energy fluxes in equation A1. The seasonal amplitude (the amplitude of the annual Fourier harmonic in phase with the insolation) of the horizontal energy flux convergence (left panel) and the energy tendency are shown. Solid lines represent calculations that include kinetic energy; dashed lines do not include kinetic energy. All calculations were done from Fasullo and Trenberth's (2008b) study. 59

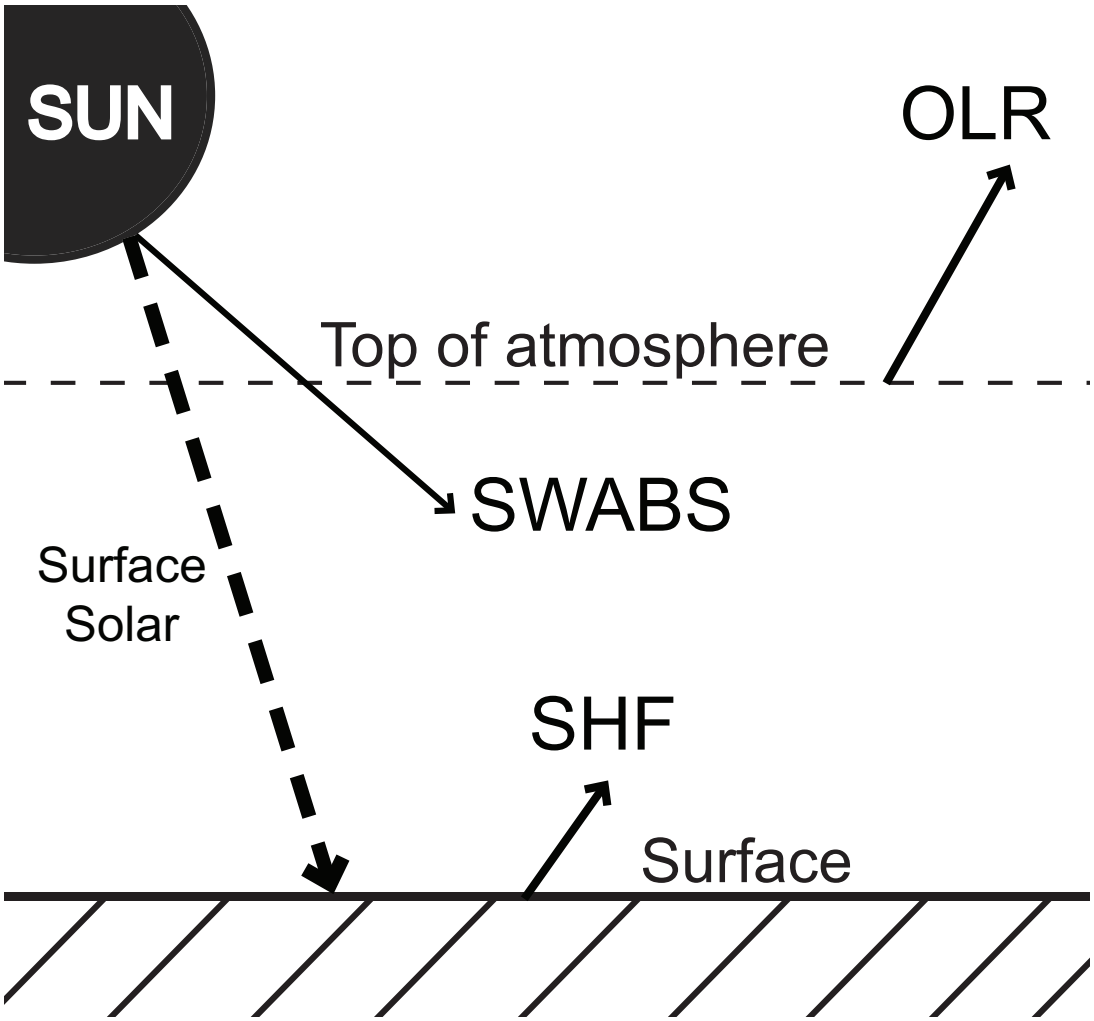

FIG. 1. Schematic of the energy exchanges between the sun, the atmosphere, and the surface. *SWABS* is the solar insolation absorbed within the atmosphere. *SHF* is the net upward energy flux from the surface to the atmosphere. *OLR* is the outgoing longwave radiation at the top of the atmosphere. The surface solar fluxe (dashed line) is the solar flux to the surface and does not enter the atmospheric energy budget because this radiation passes through the atmosphere.

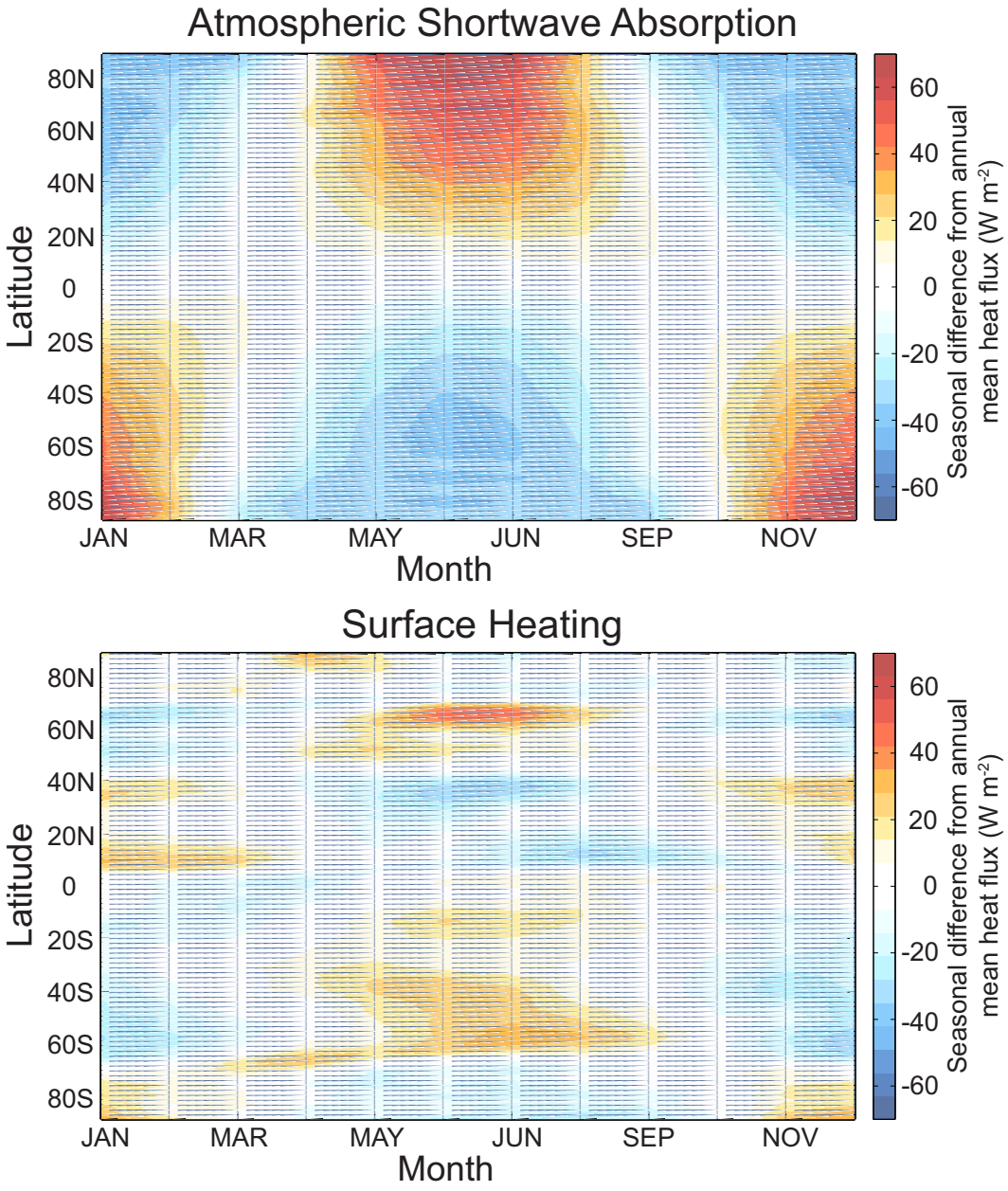

FIG. 2. Observed zonal mean seasonal cycle of atmospheric heating by atmospheric solar absorption (*SWABS* – top panel) and by upward surface heat fluxes (*SHF* – bottom panel) in W m^{-2}. The annual average at each latitude has been removed. The atmospheric solar absorption is calculated from the CERES data at the TOA and surface and the surface heating is calculated from the residual of the terms in Equation 1 as discussed in the text.

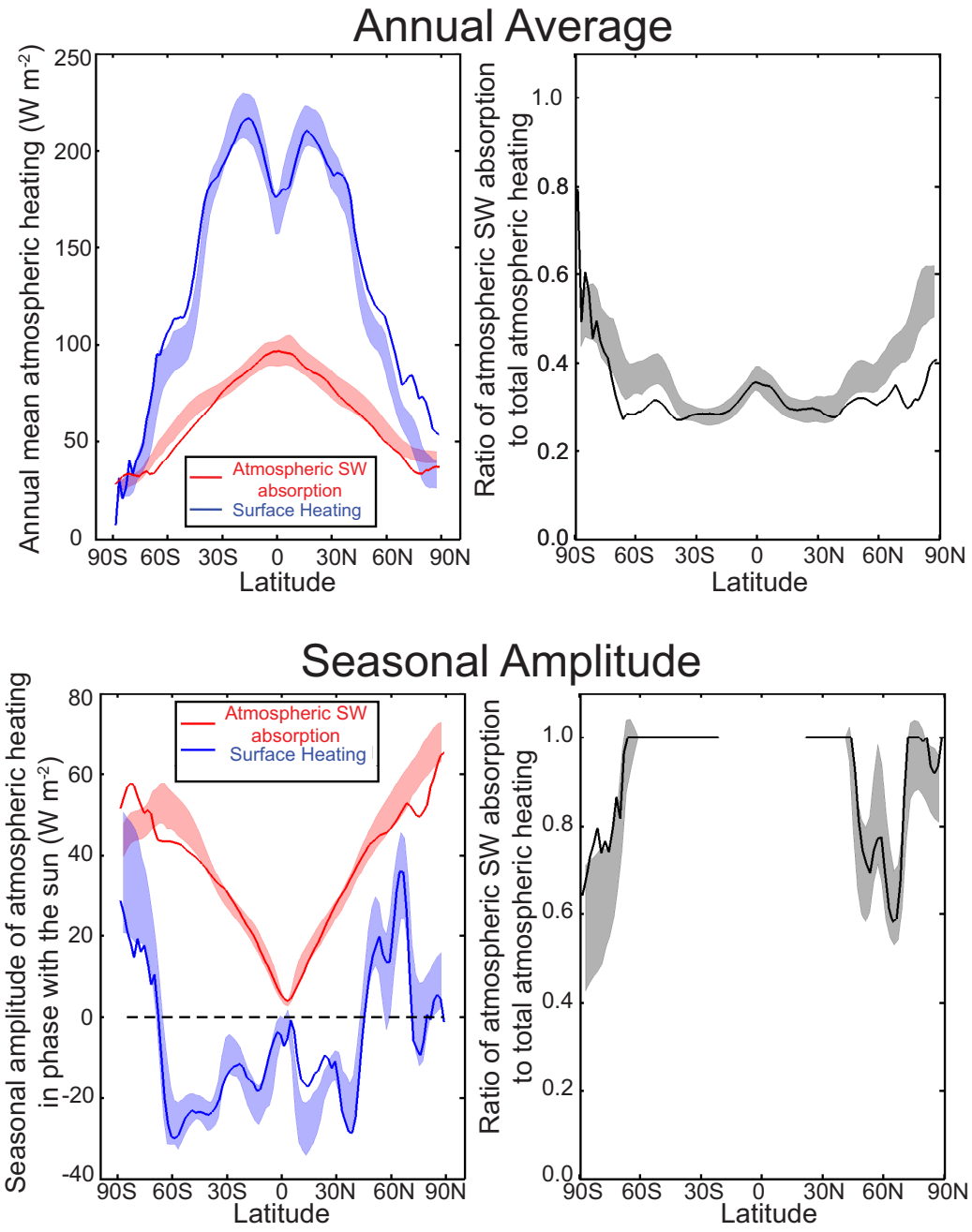

FIG. 3. Zonal mean heating of the atmosphere in the annual average (top panel) and in the seasonal cycle (bottom panel). The heating is divided into atmospheric shortwave absorption (SWABS, red) and upward surface fluxes (blue). The right panels show the fractional contribution of SWABS to the total heating (defined as $SWABS$ / ($SWABS$ + $H(SHF)$) where H is the Heaviside function and the tropics are excluded from the seasonal calculation. The seasonal amplitude is defined throughout as the amplitude of the Fourier harmonic in phase with the sun. In each figure, the solid line is the observations and the shading is $\pm 1\sigma$ about the ensemble mean pre-industrial simulations from the CMIP3 models.

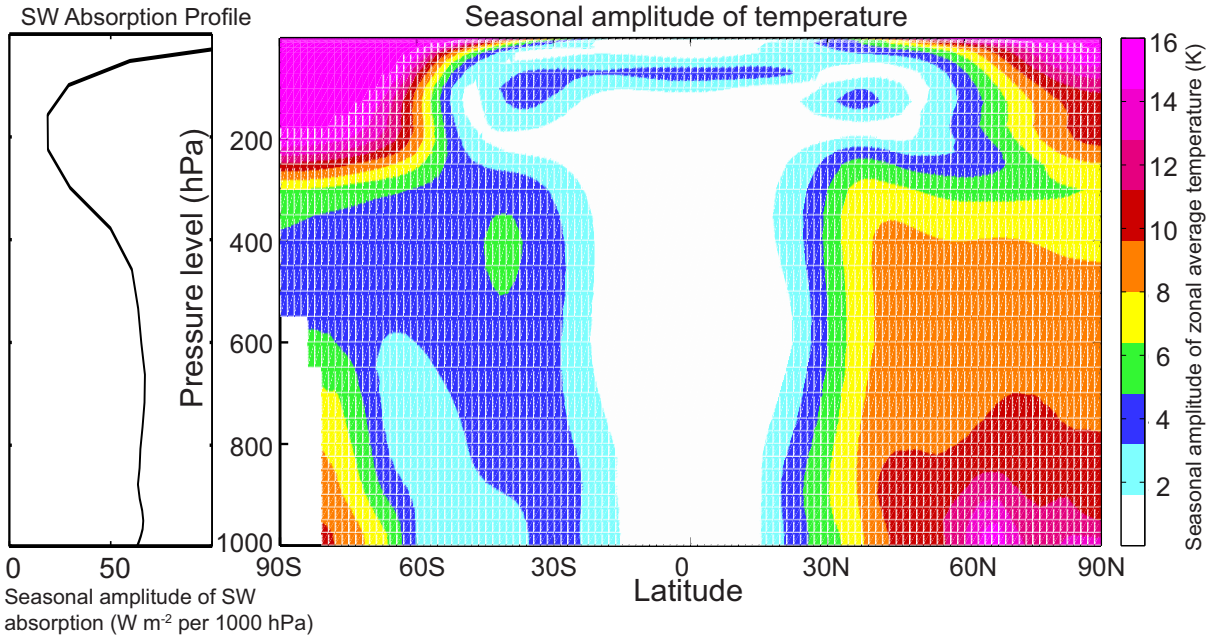

FIG. 4. (Left panel) The vertical distribution of the seasonal amplitude of *SWABS* averaged over the extratropics from a pre-industrial simulation of the GFDL 2.1 model. (Right panel) The observed zonal mean seasonal amplitude of temperature.

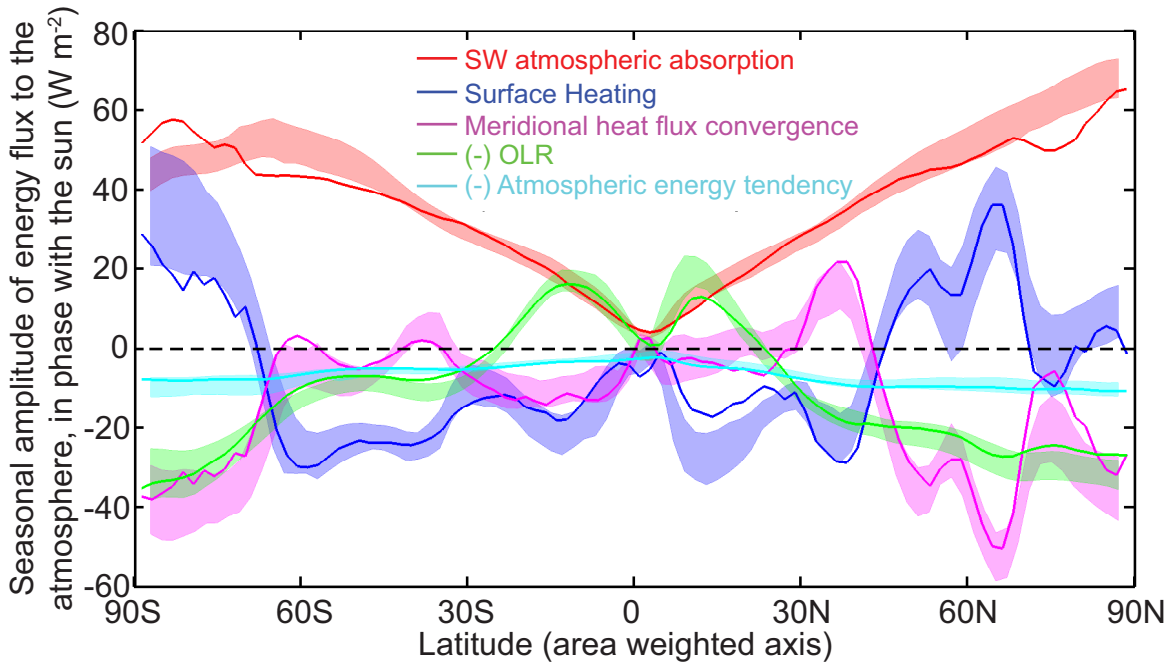

FIG. 5. The seasonal amplitude of atmospheric energy fluxes in phase with the sun (positive fluxes amplify the seasonal cycle, negative fluxes reduce the seasonal cycle). Solid lines are observations and shaded regions represent $\pm 1\sigma$ about the ensemble mean pre-industrial simulations from the CMIP3 models.

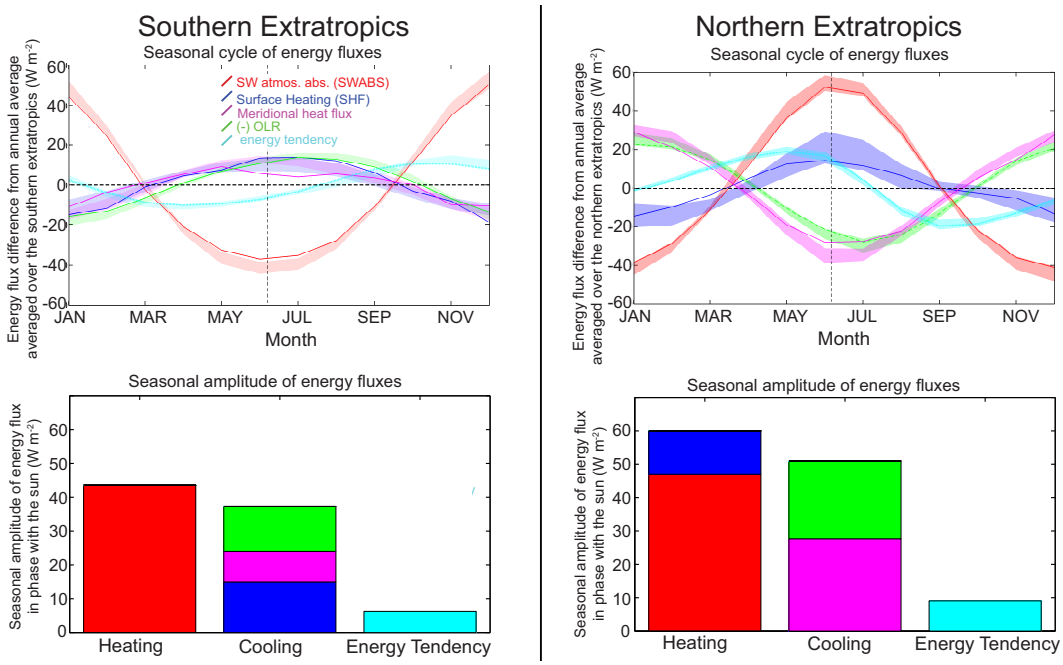

FIG. 6. (top panel) The seasonal cycle of atmospheric energy fluxes(in W m^{-2}) averaged over the extratropics – defined as poleward of 42°– in the southern hemisphere (left panel) and the northern hemisphere (right panel). The observations are shown by the solid lines and the shaded region represents $\pm 1\sigma$ about the CMIP3 PI ensemble average. The dashed vertical lines represent the winter solstice in the SH plot and summer solstice in the NH plot. The annual average of each term has been removed. (bottom panel) The seasonal amplitude of the atmospheric energy fluxes in phase with the seasonal cycle of solar insolation averaged over the extratropics (the left panel is the southern extratropics and the right panel is the northern extratropics). The terms that amplify the seasonal cycle in temperature (heating) are in the first column. The seasonal energy loss terms (cooling) are in the second column. The third column is the energy stored in the atmospheric column (energy tendency). The individual terms are color coded in the legend in the upper left panel and explained in the text.

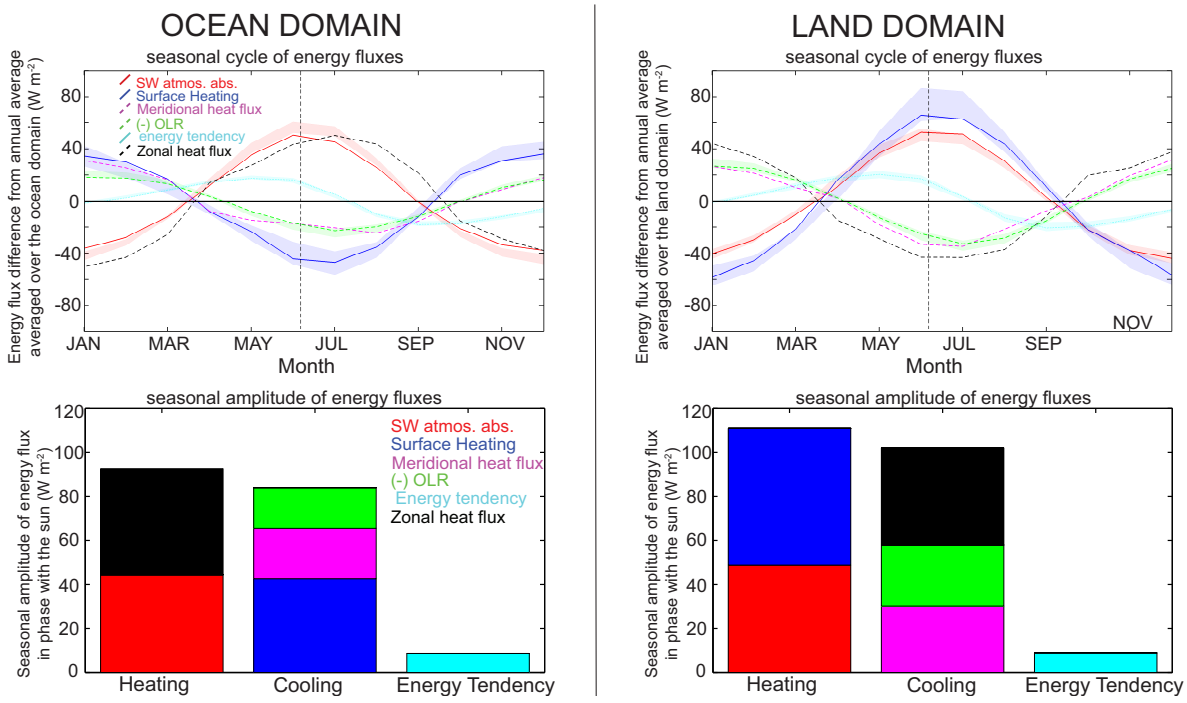

FIG. 7. (top panels) The seasonal cycle of energy fluxes averaged over the atmosphere in the NH extratropical ocean domain (left panel) and land domain (right panel). Observations are given by solid lines and the shading represents 1 of the CMIP3 pre-industrial ensemble. The atmospheric heat fluxes are decomposed into zonal and meridional components in the observations. The vertical dashed line represents the summer solstice. (bottom panels) The seasonal amplitude of energy fluxes (in phase with the sun) averaged over the ocean/land domains. The amplifying fluxes are on the left and the damping (i.e, out of phase fluxes) are in the middle (colors are described in the legend).

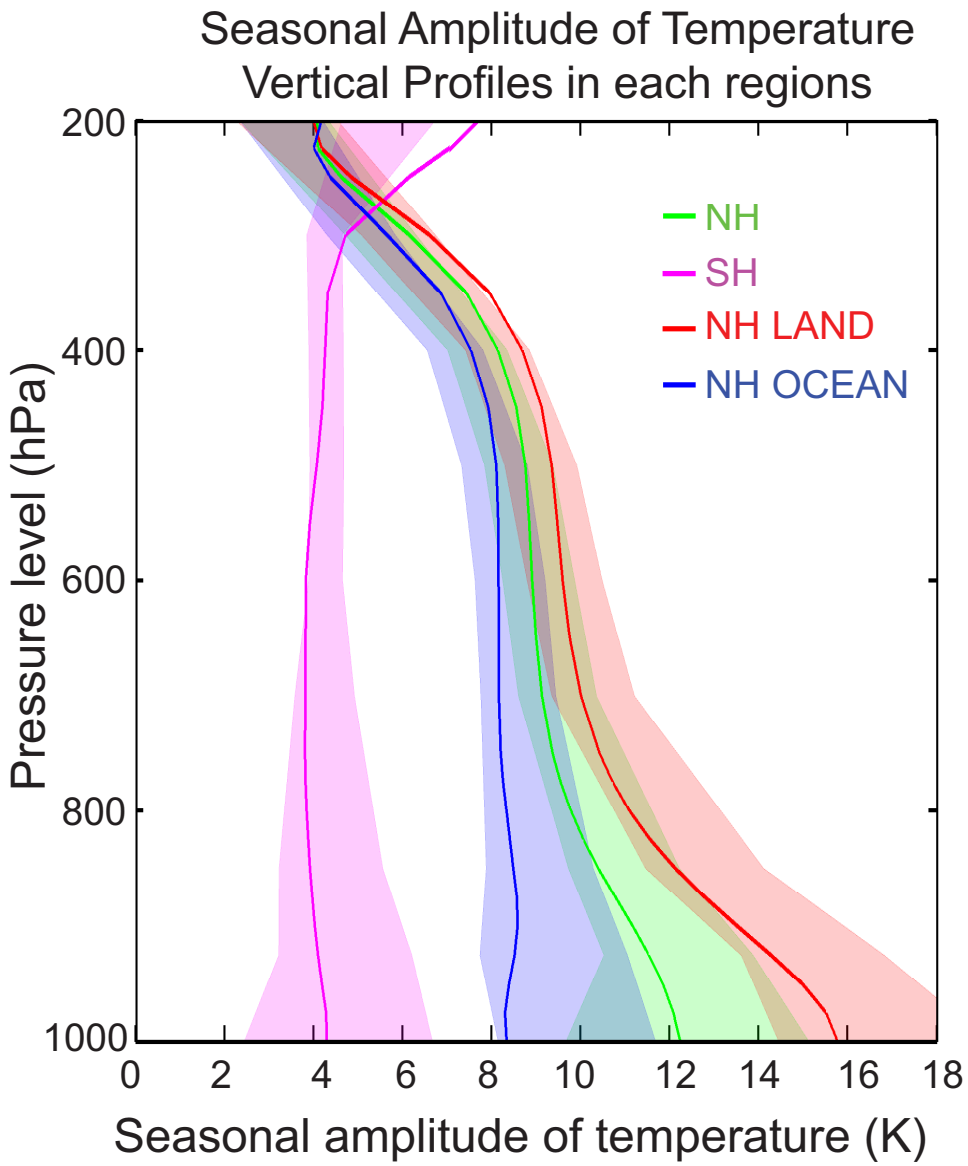

FIG. 8. The seasonal amplitude of temperature averaged over the extratropics (poleward of 42°) in each hemisphere (in K). The northern extratropics is further decomposed into ocean and land domains. The observations are given by the solid line and the shading represents $\pm 1\sigma$ about the ensemble mean pre-industrial simulations from the CMIP3 models.

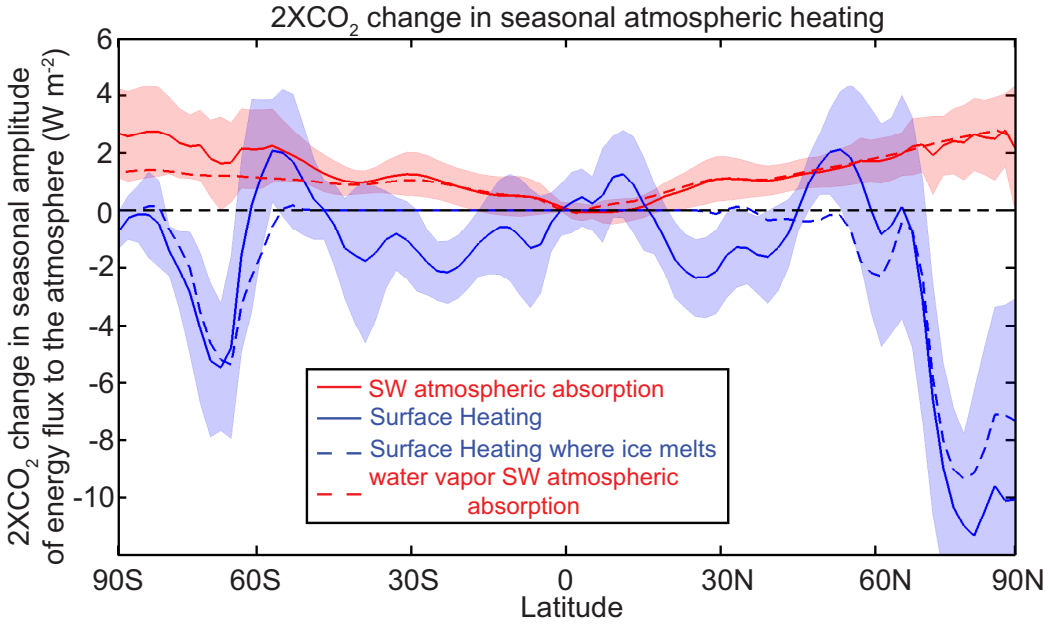

FIG. 9. The change in the seasonal amplitude of atmospheric heating in the CMIP3 CO_2 doubling experiment. The solid red line is the ensemble average change in *SWABS*, the shaded red area is $\pm 1\sigma$ of the model response and, the dotted red line is the change due to water vapor changes as diagnosed from the water vapor shortwave kernel. The blue line is the change in the seasonal amplitude of *SHF* (with shading $\pm 1\sigma$) and the dotted blue line is the change within the sub portion of the latitude band where the sea ice fraction decreases by more than 10% relative to the PI simulation.

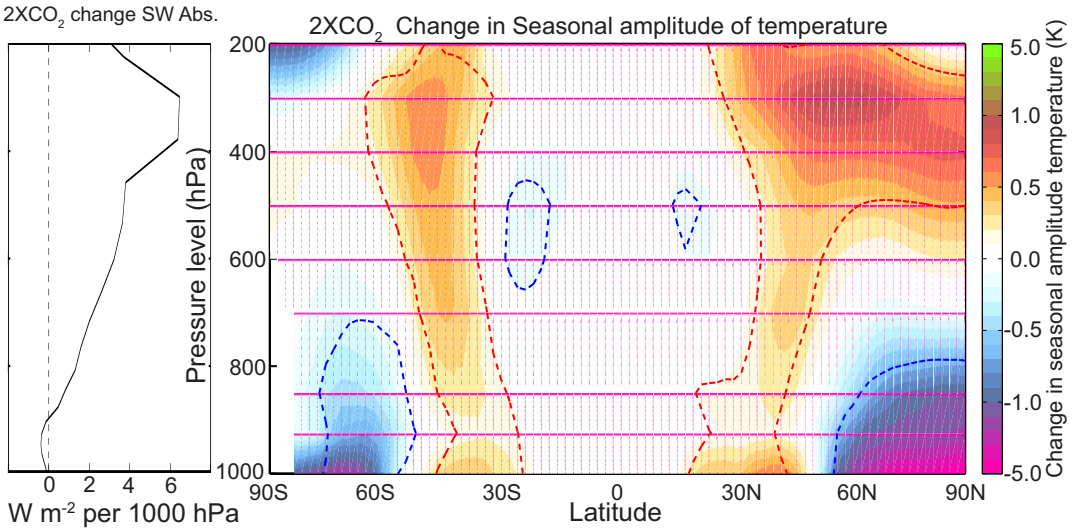

FIG. 10. (Right Panel) Zonal and ensemble average change in the seasonal amplitude of temperature in the CMIP3 CO_2 doubling experiments. The contours show the regions of significant change as assessed by a one sample t-test at the 99% confidence interval. (Left Panel) The vertical profile of the change in the seasonal amplitude of shortwave radiative heating in the GFDL 2.1 CO_2 doubling experiment expressed as the change in column integrated *SWABS* in W m^{-2} that would result if that heating rate were vertically invariant over the entire column.

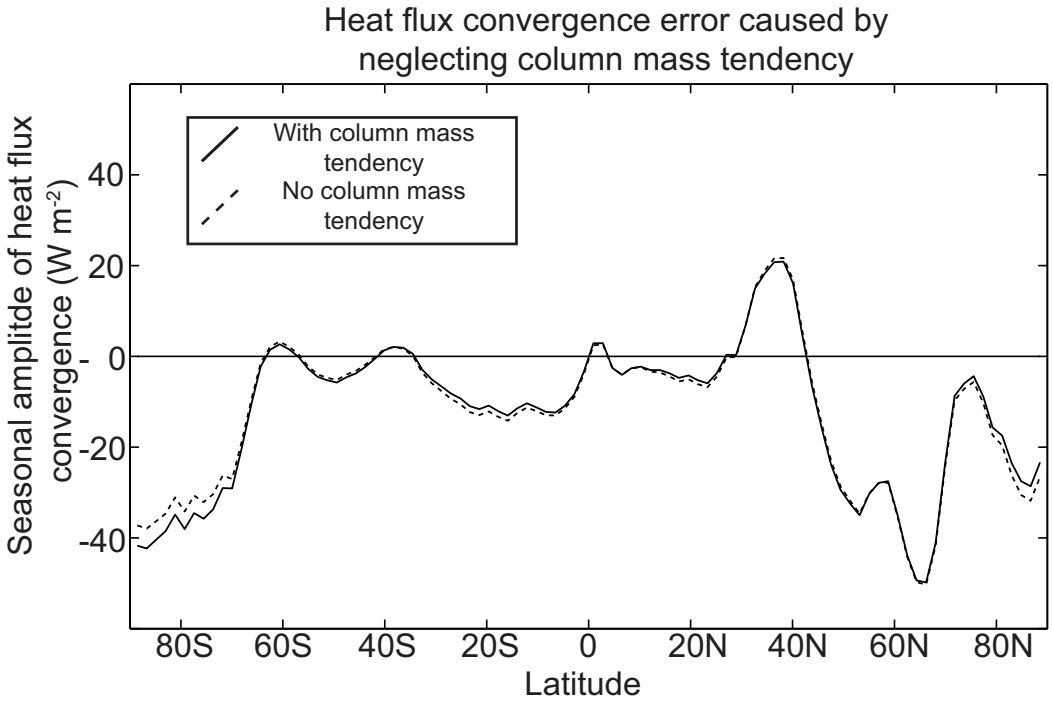

FIG. 11. Effect of neglecting the mass column tendency on the energy flux calculations presented in this manuscript. The solid line is the seasonal amplitude of the zonal average energy flux convergence using all terms and the dashed line is the same calculation neglecting the column mass tendency term (first term in Equation A5).

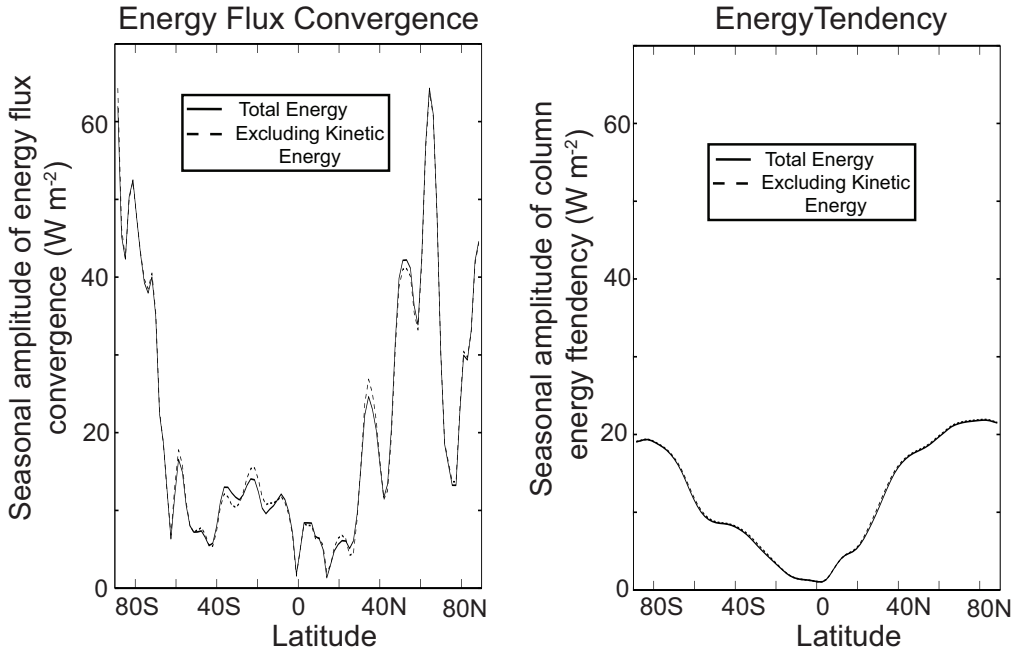

FIG. 12. Effect of neglecting the kinetic energy on the energy fluxes in equation A1. The seasonal amplitude (the amplitude of the annual Fourier harmonic in phase with the insolation) of the horizontal energy flux convergence (left panel) and the energy tendency are shown. Solid lines represent calculations that include kinetic energy; dashed lines do not include kinetic energy. All calculations were done from Fasullo and Trenberth's (2008b) study.